# MACHINE LEARNING APPROACH TO ISLANDING DETECTION FOR INVERTER-BASED DISTRIBUTED GENERATION

A Dissertation

by

BILJANA MATIC CUKA

Submitted to the Office of Graduate and Professional Studies of
Texas A&M University
in partial fulfillment of the requirements for the degree of

DOCTOR OF PHILOSOPHY

| | |
|---|---|
| Chair of Committee, | Mladen Kezunovic |
| Committee Members, | Karen Butler-Purry |
| | Alex Sprintson |
| | Erick Moreno-Centeno |
| Head of Department, | Chanan Singh |

December 2014

Major Subject: Electrical Engineering

# ABSTRACT

Despite a number of economic and environmental benefits that integration of renewable distributed generation (DG) into the distribution grid brings, there are many technical challenges that arise as well. One of the most important issues concerning DG integration is unintentional islanding. Islanding occurs when DG continues to energize portion of the system while being disconnected from the main grid. Since the island is unregulated, its behavior is unpredictable and voltage, frequency and other power system parameters may have unacceptable levels, which may cause hazardous effect on devices and public. According to the IEEE Standard 1547 DG shall detect any possible islanding conditions and cease to energize the area within 2 sec.

In this dissertation work, a new islanding detection method for single phase inverter-based distributed generation is presented. In the first stage of the proposed method, parametric technique called Autoregressive (AR) signal modeling is utilized to extract signal features from voltage and current signals at the Point of Common Coupling (PCC) with the grid. In the second stage, advanced machine learning technique based on Support Vector Machine (SVM) which takes calculated features as inputs is utilized to predict islanding state. The extensive study is performed on the IEEE 13 bus system and feature vectors corresponding to various islanding and non-islanding conditions, such as external grid faults and power system components switching, are used for SVM classifier training and testing. Simulation results show that proposed

method is robust to external grid transients and able to accurately discriminate islanding conditions 50ms after the event begins.

DEDICATION

To my family.

ACKNOWLEDGEMENTS

I would like to express my sincere gratitude to my advisor Dr. Mladen Kezunovic for his support and guidance throughout my studies at Texas A&M University. His knowledge and experience contributed many of the inspiring ideas explored in this dissertation.

I gratefully thank my committee members Dr. Karen Butler-Purry, Dr. Alex Sprintson, and Dr. Erick Moreno-Centeno for their time, comments and support. I would like to thank Dr. Le Xie for his time and comments. Also, I would like to acknowledge contribution of Dr. William M. Lively who had significant impact on this dissertation work. Thanks also go to my friends and colleagues and the department faculty and staff for making my time at Texas A&M University a great experience.

Sincere acknowledgements are extended to my colleagues, Mr. Jinfeng Ren, Mr. Yufan Guan, Mr. Ce Zheng, Mrs. Yimai Dong, Mrs. Papiya Dutta, Mr. Saeed Lotfifard, Mr. Chengzong Pang, Mr. Vuk Malbasa and other group members for their corporation and assistance. It was a most enjoyable experience in my life working with them.

Funding for this research was provided by the U.S. DOE's Office of Electricity Delivery and Energy Reliability under the project "The Future Grid to Enable Sustainable Energy Systems." conducted through NSF I/UCRC Power Systems Engineering Research center (PSerc). Also I would like to acknowledge the financial support from the Vestas for the opportunity to work on the project "Impact of Wind Power Generation on Protection System" and EPRI, CenterPoint Energy, HydroOne,

AEP-Texas, FirstEnergy, TXU Delivery for funding my work on the “Multiple Uses of Substation Data” project.

# NOMENCLATURE

| | |
|---|---|
| AC | Alternating current |
| AFD | Active Frequency Drift |
| AR | Autoregresive |
| APS | Automatic Phase Shift |
| C | Capacitance |
| C_p | Penalty Factor |
| DC | Direct Current |
| DG | Distributed Generation |
| DWT | Discrete Wavelet Transform |
| ESPRIT | Estimation Signal Rarameter via a Rotational Invariant Technique |
| f | Frequency |
| FERC | Federal Energy Regulatory Commission |
| FFT | Fast Fourier Transform |
| $\gamma$ | SVM kernel parameter |
| HCP | Hierarchical Coordinated Protection |
| HVDC | High Voltage Direct Current |
| I | Current |
| IEC | International Electrotechnical Commission |
| IED | Intelligent Electronic Device |
| IEEE | Institute of Electrical and Electronics Engineers |

| | |
|---|---|
| L | Inductance |
| LIBSVM | Library for Support Vector Machines |
| LVR | Low Voltage Ride |
| NDZ | Non-detection Zone |
| NN | Neural Networks |
| OFR | Over Frequency Relay |
| OVR | Over Voltage Relay |
| P | Active Power |
| PCC | Point of Common Coupling |
| PID | Proportional-Integral-Derivative |
| PLL | Phase-Locked Loop |
| PSD | Power Spectral Density |
| PV | Photovoltaic |
| Q | Reactive Power |
| Q_f | Quality Factor |
| R | Resistance |
| RBF | Radial Bias Function |
| SFS | Sandia Frequency Shift |
| RMS | Root Mean Square |
| SRM | Structural Risk Minimization |
| SVM | Support Vector Machine |
| UFR | Under Frequency Relay |

| | |
|---|---|
| UVR | Under Voltage Relay |
| V | Voltage |

TABLE OF CONTENTS

Page

LIST OF FIGURES

Page

LIST OF TABLES

Page

# CHAPTER I

# INTRODUCTION

## 1.1. Background

The rise in the energy demand, environmental concerns and favorable government policies have introduced new directions and challenges in the power grid development. The conventional grid is the network with a few large, centralized generation sources at the transmission system that supplies passive users at distribution system. This is drifting away towards the network with many renewable distributed generation (DG) sources at all voltage levels, see Figure1. Since power system structure and philosophy are changing the existing practices for managing power system congruencies and maintaining power system operation may struggle to cope with new conditions caused by DG integration. Besides benefits of integration such as environmental and economic benefits, load peak shaving, infrastructure upgrades deferral, energy losses and upstream congestion reduction, there are many adverse effects on power system integrity and new challenges arise in the areas of power system control, operation and protection.

The effect of dispersed energy sources integration on the power system operation and reliability depends mainly on DG type and technology, size and interconnection point. And the biggest challenge for utility personnel is to make sure that DGs operate in

safe environment and that their connections/disconnections will not worse grid integrity. DG integration into the power grid may have negative impact on: system stability and

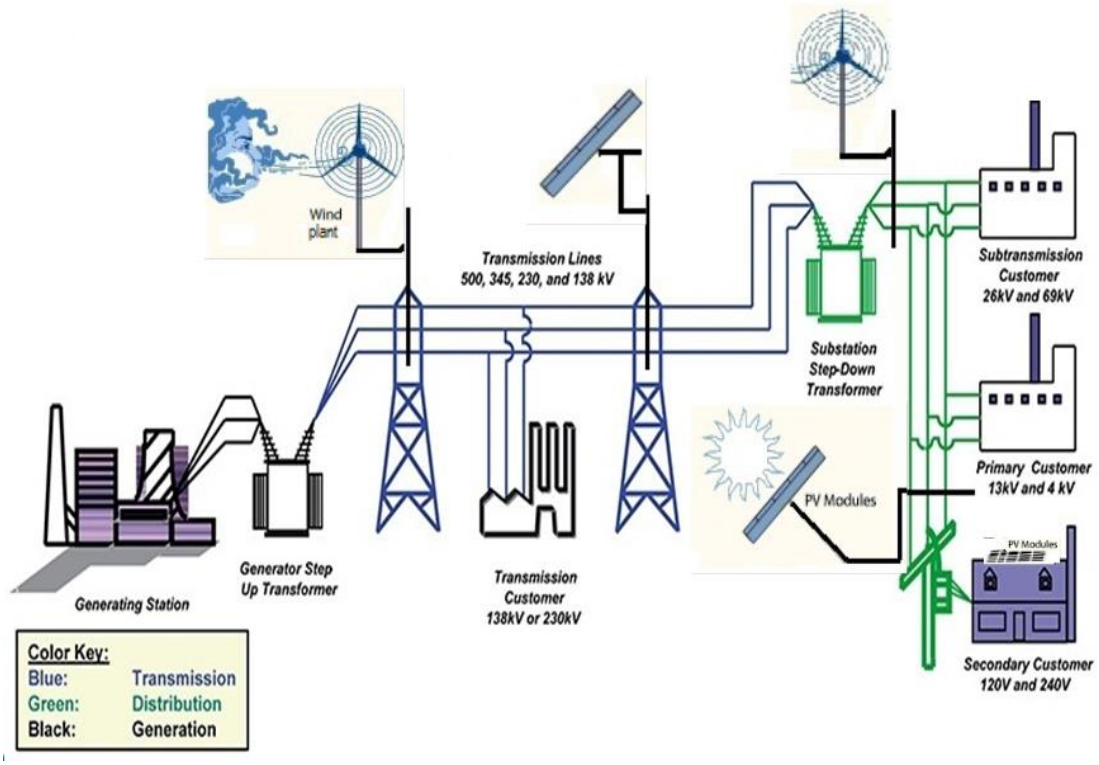


Figure 1 Basic Structure of the Power System

voltage regulation due to sudden load change, existing protection practices due to varying short circuit current levels, power quality due to variable nature of the energy sources, and it may energize a portion of the system that is disconnected from the main grid causing unintentional islands. To reduce and regulate impacts of DG integration many countries and utility companies have established guidelines while the International

Electrotechnical Commission (IEC), the Institute of Electrical and Electronics Engineers (IEEE) and other standard bodies have been formulating interconnection standards.

In the last decade due to significant development in the power electronics and digital control technology, a number of large scale, offshore and onshore wind generation units and farms have been installed in the transmission system. In the attempt to maintain reliability of the transmission grid with high wind energy penetration Federal Energy Regulatory Commission (FERC) proposed low voltage ride (LVR) through the fault requirements in Order 661-A [1]. This requirement implies that wind energy sources should stay connected to the grid during most disturbances and should continue to energize interconnection area to prevent sudden system load changes. Disconnection of high penetration wind energy sources may cause incorrect operation of the relays followed by system wide disturbances and system stability problems at transmission level due to sudden increase in the load.

According to Order 661-A wind plant should stay connected to the transmission system for a grid disturbances resulting in voltage drop up to 85% for 625ms time period. Further, the wind plant should stay connected if voltage returns to 90% of the rated value within 3s from the beginning of the voltage drop, see Figure 2. It is also required that the wind plant shall maintain power factor in range of 0.95 leading to 0.95 lagging at the point of interconnection.

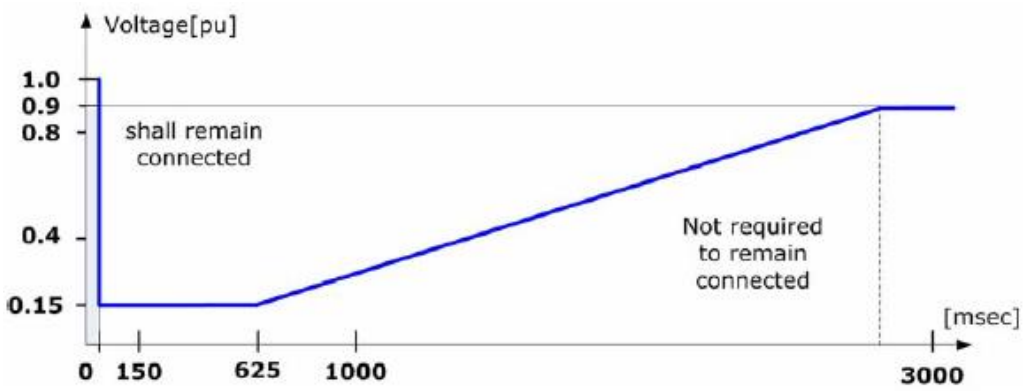


Figure 2 Required Wind Plant Response to Emergency Low Voltage by FERC 661-A [2]

On the other hand, the photovoltaic (PV) systems began to evolve recently when the cost of power electronic inverters decreased and PVs found broad applications at the distribution level as small residential units. In order to maintain integrity of distribution grid with small scale DG penetration IEEE-1547 standard [3] is proposed. The IEEE-1547 requirements are applicable for DGs in 60 Hz system with generation capacity less than 10MW and they should be met at the point of common coupling with the power grid. The main idea of IEEE-1547 is that DG should not affect operation, protection and power quality of the distribution system and that it should be quickly disconnected under abnormal conditions. The standard does not allow inverter-based DG control capabilities utilization and it prohibits voltage regulation and reactive power generation. In the case of the islanding, standard requires fast DG disconnected form the system.

## 1.2 Existing and Future Causes of Protection System Deterioration

Over the time, the transmission system structure has become more complex and operation scenarios have changed due deferral of the grid infrastructure upgrade. The system has been planned to operate with tighter margins, less redundancy, reduced system inertia and fault levels, and under exemplified dynamic grid operating phenomena such as power and voltage oscillations, as well as voltage, frequency and angular instability. These phenomena may cause new dynamic behavior in the typical protection measurements such as voltage, current, frequency, power, etc. Such changes in the measurement properties may deteriorate protection system performance leading to unintended operation or mis-operation.

In addition, installation of DG at the distribution level changes the distribution system behavior from passive network that transfers power from substation to the customers in a radial fashion to an active network with generation sources causing bidirectional flows. This change may affect protection coordination and selectivity or may cause unintentional islanding.

These new phenomena may affect protective relaying dependability, security, selectivity and speed. The dependability is defined as the degree of certainty that relay will operate correctly for the faults in the protection zone. The security is defined as a relay characteristics not to operate for non-fault disturbances, such as component switching, line overloading, swing condition, ect. The selectivity is relay characteristics to disconnect only faulted element from the system and minimize fault affected area.

The relay decision speed may be affected by the system inertia and complexity. In some cases additional signal processing is required to make sure that relay is operating correctly to prevent unintentional tripping due to non-fault disturbances.

To design protection method that has good dependability and security characteristics is challenging. And, in the past, protection methods were designed to operate with the bias toward dependability. However recently it was recognized that security has the equal importance to achieve effective and reliable protection operation.

New power system behaviors that arise due to integration of DGs into the power system network and may have an impact on power system protection and conventional relaying practice may be summarized as:

- bidirectional power flows that needs to accommodate,
- new generator technology that may limit/increase the fault currents
- islanded mode of operation

The following sections give more details about the issues that may arise in the system with DG penetration:

### *1.2.1 Reverse Power Flow*

Introducing DGs at the load side have many benefits. They may provide some or all of the required power for the demand increase and reduce the load demand. Simultaneously, this leads to reduction in line losses and improvement in voltage profiles and overall system performances. This statement is true, as long as the DG

generation matches with the substantial load demand so that the net power flow remains going from the substation to the load side. However, as the penetration levels of DGs rise, there may be time periods during the day when DGs' energy production is higher than the local demand causing the power flow to change its direction from the load towards the substation. This situation is not normally anticipated in the power system design and it will affect performance of the distribution feeder standard protection schemes with directional overcurrent relays.

### *1.2.2 Short Circuit Level*

Connection of DG into power grid has various impacts on the performance of the existing protection schemes. The impact depends on DG type, size and location, impedance and configuration of the line. DGs contribute current to the circuit and their contribution may rise, lower or change direction of the short circuit (SC) current. Machine based DGs injects SC current levels of more than 5 times their rated current and may contribute to the short circuit current for long time due to high inertia. On the other head, the inverter based DGs have lover contribution up to 2 times rated current and trip off very quickly due to low inertia.

If, for example we take a look at SC current level in the system without conventional generation, such as collector system of an offshore wind plant connected to the transmission grid trough high voltage direct current (HVDC) link and analyze whether conventional protection practices may be applicable, see Figure 3,

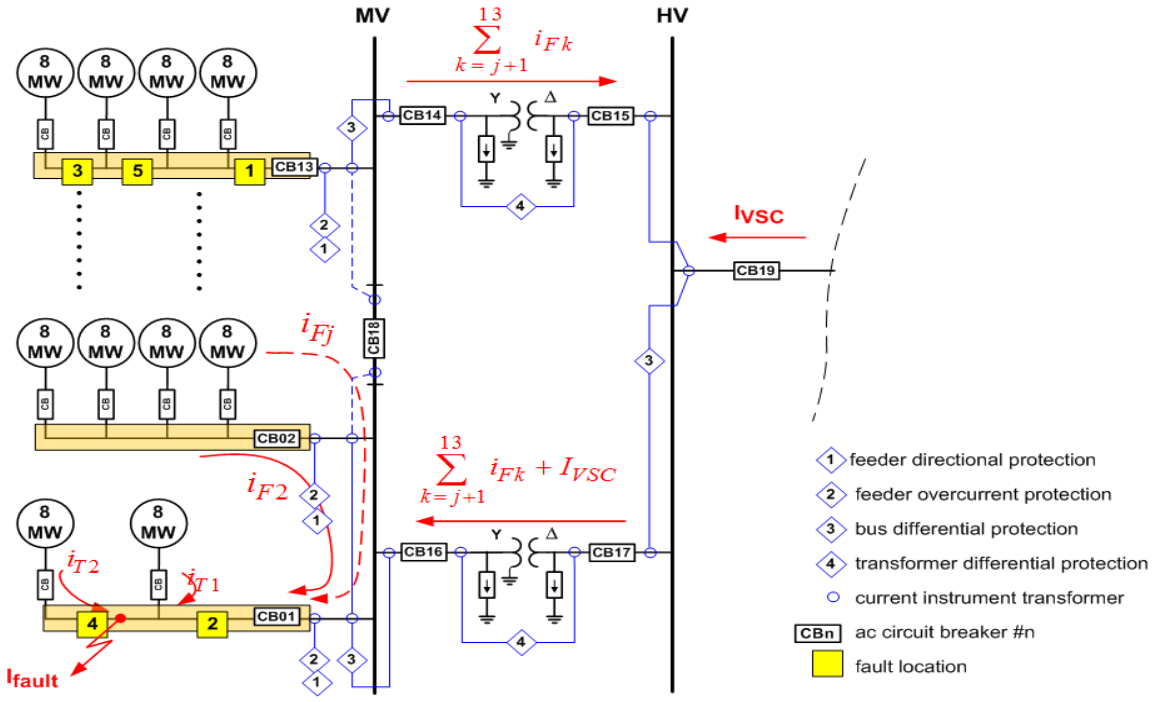


Figure 3 Offshore Wind Plant

In the case of the fault, SC current contribution from the Full Converter Wind Turbine Generator (WTG) is less than 1.2 pu and SC contribution from the grid is less than 1.5 pu due to HVDC converters see Figure 4. We may see that SC level for the ground fault at the feeder is too low that it cannot be detected by the standard Overcurrent protection and that more sophisticated solutions are required.

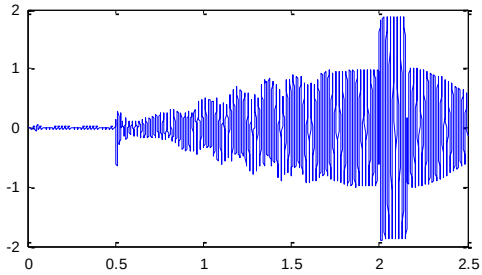


Figure 4 Phase A Current at Beginning of the Faulted Feeder for AG fault

The similar situation is in a remote parts of a distribution network equipped with inverter based DG installations, it could happen that in case of a failure there is almost no significant rise of the phase current and the fault is therefore not detected by the overcurrent protection system.

### *1.2.3 Islanded Mode of Operation*

The islanding occurs when DG continues to energize a portion of the system while being disconnected from the main grid. Since the island is unregulated, its behavior is unpredictable and voltage, frequency and other power system parameters may have unacceptable limits. The out-of-phase reclosing is possible and high transient inrush currents may damage local devices. Also unintentional islanding in the system may create electric shock if energized conductors that are assumed to be disconnected are touched by public or utility workers. Thus, the islanded systems should be de-energized promptly.

According to the IEEE Standard 1547 DG shall detect the islanding for any possible islanding conditions and cease to energize the area within 2 sec for small voltage signal variations at PCC, while for large voltage changes below 0.50 pu or above 1.2 pu and all frequency variations islanding should be detected within 0.16 s, see Table I.

Table I DG System Response to Abnormal Voltages

| IEEE Standard 1547 | |
|---|---|
| Voltage Range (%) | Disconnection Time ( s) |
| $V \leq 50$ | 0.16 |
| $50 \leq V \leq 88$ | 2 |
| $110 < V < 120$ | 1 |
| $V \geq 120$ | 0.16 |

In this study the islanding phenomenon is analyzed and novel islanding detection method that has equal bias toward dependability and security is proposed. In the next section the islanding problem is described in the detail.

## 1.3 Problem Formulation

The islanding occurs when a section of the power system is accidentally disconnected from the main grid while being energized by the local DG, see Figure 5. Since, islanded system operates without utility supervision; the values of the power system parameters, such as voltage and frequency are unpredictable. Their new operating points satisfy balances of active and reactive power between the DG and the local load, which determines severity of the islanding condition. The active and reactive power mismatch is difference in active and reactive power generated by DG and consumed by the local load.

$$\Delta P = P_{DG} - P_L \tag{1.1}$$

$$\Delta Q = Q_{DG} - Q_L \tag{1.2}$$

while:

$P_{DG}$- active power generated by the DG

$P_L$- active power dissipated by the local load

$Q_{DG}$- reactive power generated by the DG

$Q_L$- reactive power dissipated by the local load

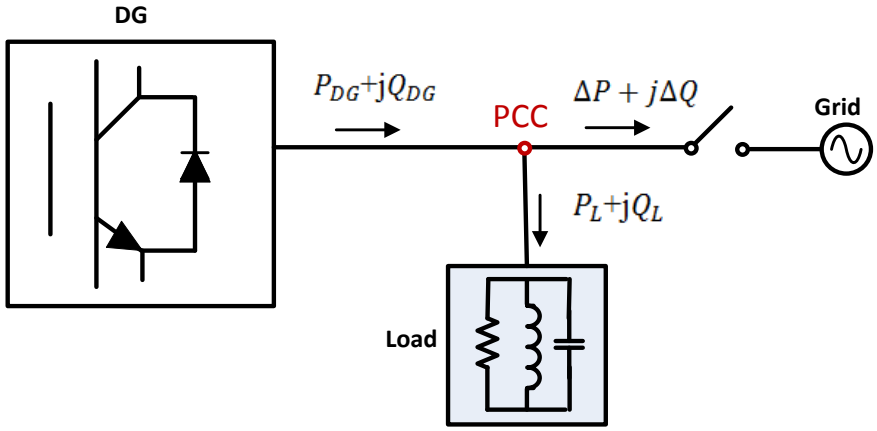


Figure 5 Islanded Power System

The local load is assumed to be parallel RLC load and active and reactive power dissipated by the load may be calculated as:

$$P_L = \frac{V^2}{R} \tag{1.3}$$

$$Q_L = V^2\left(\frac{1}{2\pi fL} - 2\pi fC\right) \tag{1.4}$$

The active power mismatch at the time of system disconnection from the grid has an effect on the voltage magnitude at PCC, while reactive power mismatch at the time of system disconnection from the grid has an effect on the frequency magnitude at PCC. Depending of the mismatches the system parameters will rise or decrease before setting to the new operating point.

In the case of positive active power mismatch (more active power is generated by DG that dissipated by the local load), voltage magnitude at PCC will increase and may stabilize at the higher level after disconnection from the grid, while for negative

active power mismatch (more active power is dissipated by the local load that it is generated by DG) voltage magnitude will decrease and may stabilize at lover value. Similarly, for positive reactive power mismatch (more reactive power is generated by DG that dissipated by the local load) frequency will decrease and may stabilize at the lower level, while for negative reactive power mismatch (more reactive power is dissipated by the local load that it is generated by DG) frequency will increase and may stabilize on the higher level. The frequency will converge to the local load resonant frequency value to keep constant power factor operation of the DG.

The most commonly used islanding detection methods are over/under-voltage protection (OVP/UVP) and over/under-frequency protection (OFP/UFP) methods. In the case of large active and/or reactive power mismatch, immediately after the disconnection voltage and frequency magnitudes will change significantly, and islanding will be detected using simple over/under-voltage and frequency relays, see Figure 6-7.

These methods are fast and simple to operate, however they are unable to distinguish islanding conditions for small active/reactive mismatches, see Figure 8-11.

Figure 6-11 shows voltage and frequency signals for different active/reactive power mismatches together with the OVR/UVR and OFR/UFR threshold limits.

The following cases are analyzed:

- *Case 1*: 50% active power mismatch, -4 % reactive power mismatch
- *Case 2:* 0% active power mismatch, 0% reactive power mismatch
- *Case 3*: -10% active power mismatch, 1% reactive power mismatch

For the Case 1 it may be observed that immediately after disconnection from the main grid voltage and frequency parameters jump above the threshold limits and stabilize at new operating points. In this case islanding will be detected using OVR/UVR and OFR/UFR. However, for the Case 1 and Case 2, rms values for voltage and frequency stay below the relays' trip thresholds and system continues to function in islanded mode of operation.

For the Case 2 frequency parameter is changing slowly and it will decrease below the threshold limit before it reaches new operating point. However, this will not be done in the timely manner, which is less than 2s, to comply with IEEE Standard 1547 requirement.

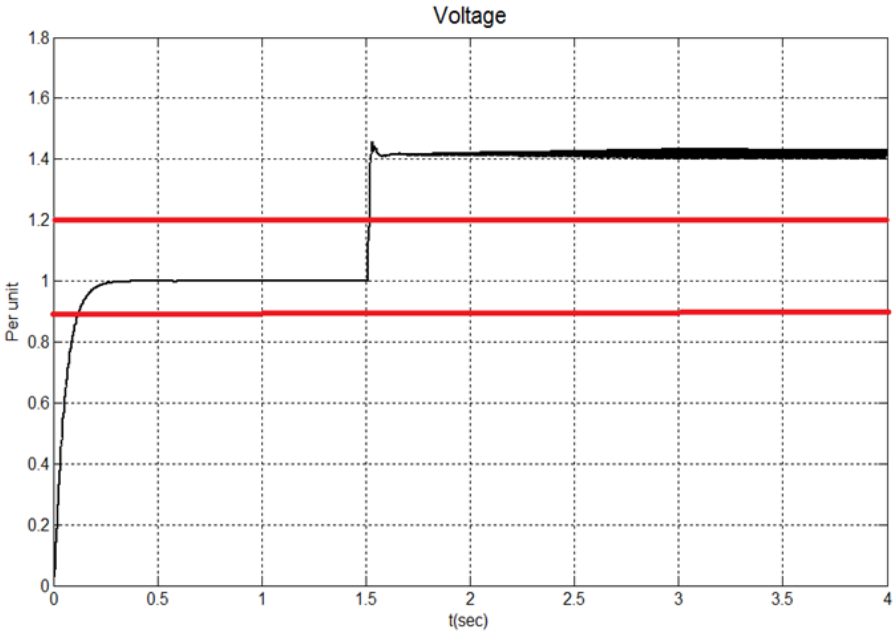


Figure 6 Case 1: Voltage at PCC for 50% Active and -4% Reactive Power Mismatch

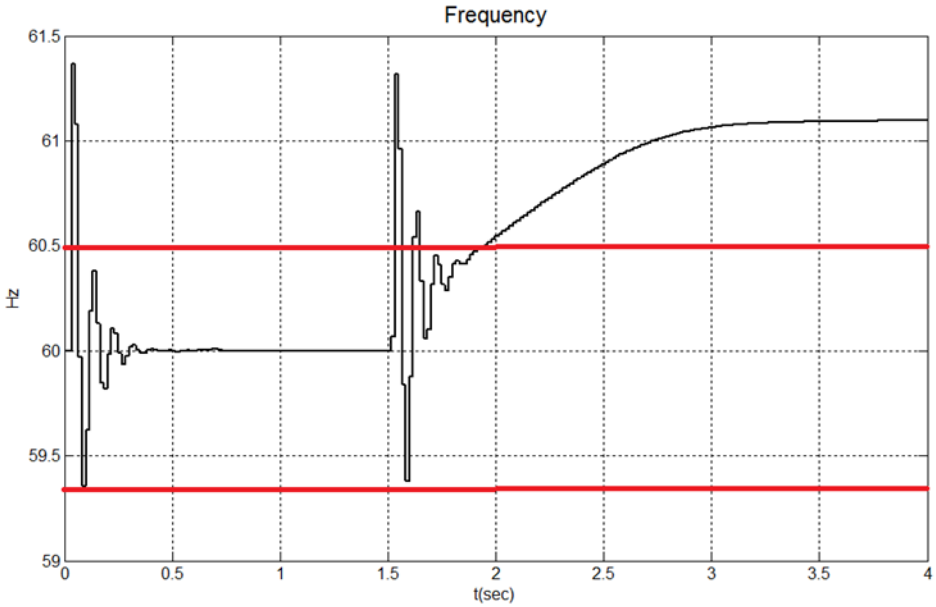


Figure 7 Case 1: Frequency at PCC for 50% Active and -4% Reactive Power Mismatch

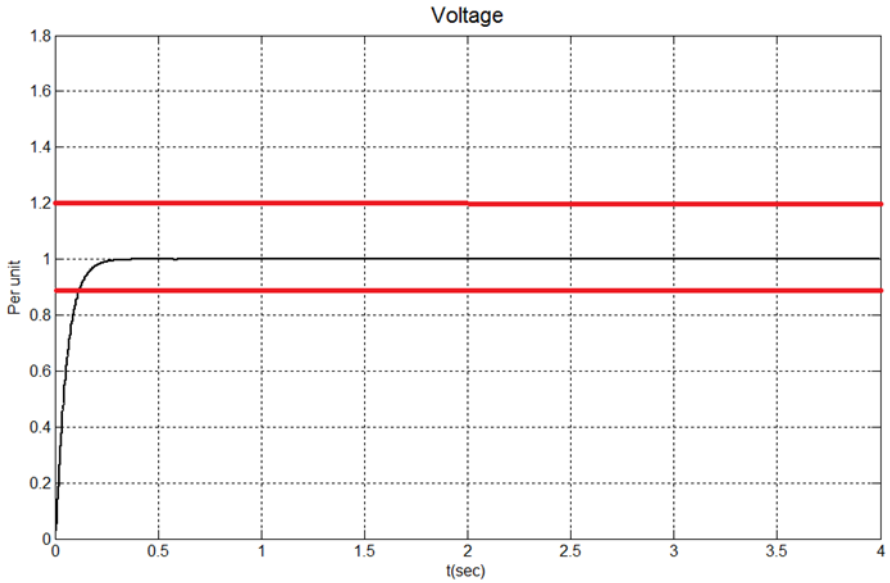


Figure 8 Case 2: Voltage at PCC for 0% Active and 0% Reactive Power Mismatch

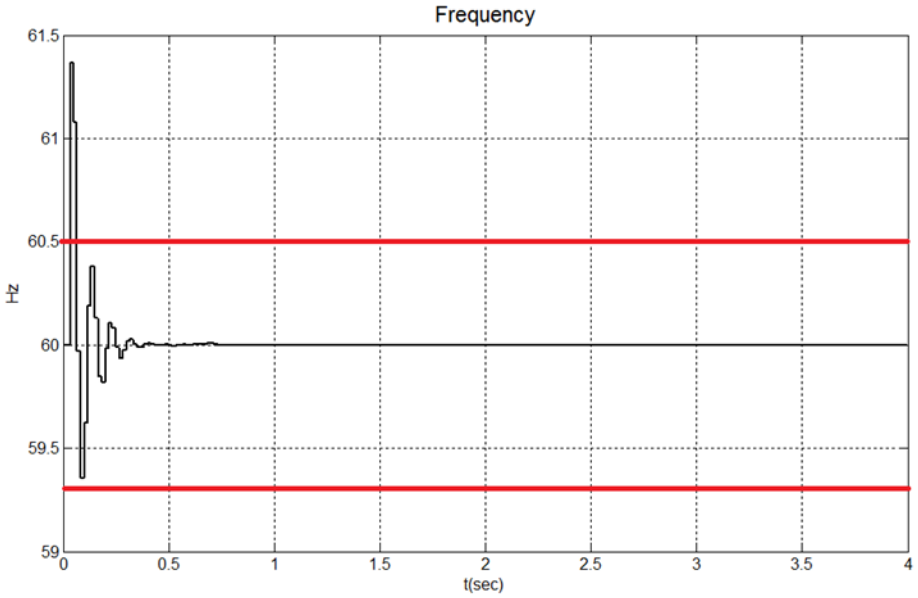


Figure 9 Case 2: Frequency at PCC for 0% Active and 0% Reactive Power Mismatch

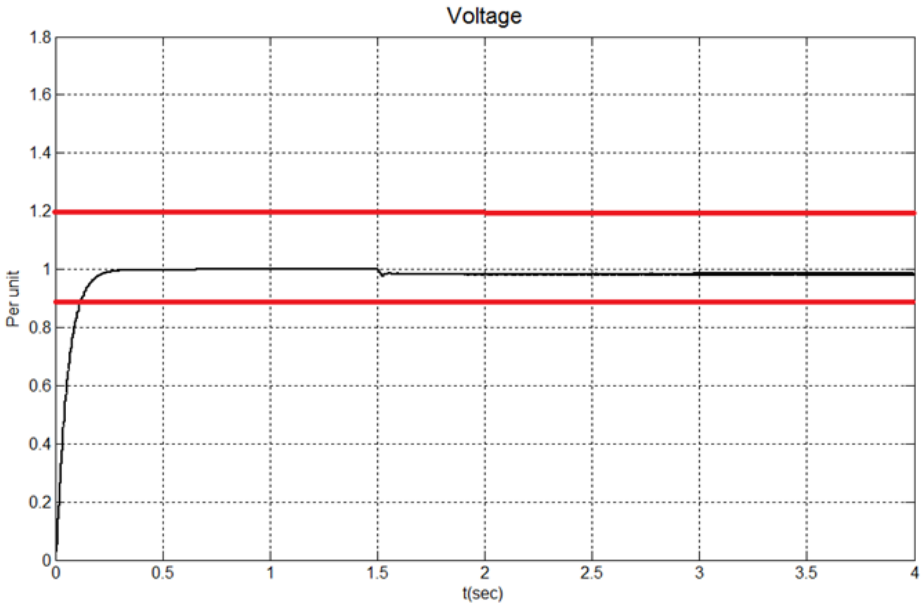


Figure 10 Case 3: Voltage at PCC for -10% Active and 1% Reactive Power Mismatch

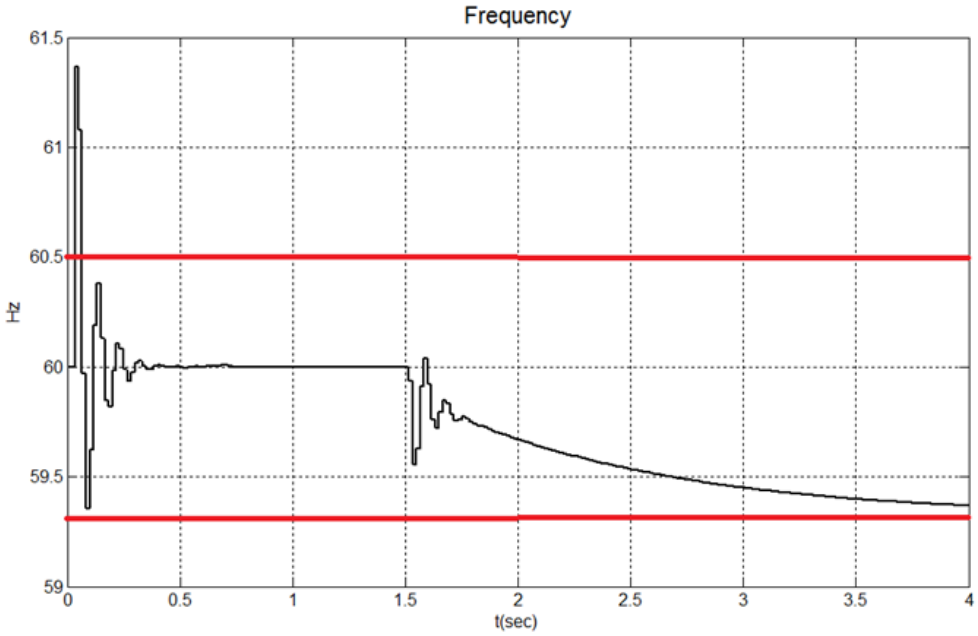


Figure 11 Case 3: Frequency at PCC for -10% Active and 1% Reactive Power Mismatch

Thus, for a smaller power mismatches, or no mismatch at all, islanding detection becomes challenging and more sophisticated methods have to be used to differentiate islanding condition.

## 1.4 Proposed Research

In this study, new anti-islanding method for single phase invertor-based DG is presented. This method uses SVM classifier to predict whether the system operates in the islanded mode. A parametric method called the autoregressive (AR) modeling is

used to extract feature vectors from voltage and current measurements at PCC and these coefficients are fed as inputs to the SVM classifier. The method is tested on the IEEE-13[4] bus system which is modeled in PSCAD/EMTDC, while MATLAB and LIBSVM [5] packages are used to extract features from the signals and to train and test the SVM models. To analyze accuracy and robustness of the proposed method a number of islanding and non-islanding events are generated. The external grid faults and component switching events, such as load, capacitor, motor and second DG switching are simulated under normal and light loading conditions.

The proposed method is based on the principle that variations in the power spectral density (PSD) functions of the voltage and current signals at PCC may be used to determine whether the DG system operates in an islanded mode. It is well known that when connected to the grid inverter-based DGs produce harmonics due to high-frequency switching, dead time and DC link voltage ripple. These harmonics are maintained by the filters and inverter embedded control solutions and should be kept below 5% for the current signal according to IEEE Standard 1547.

The magnitude of the harmonics in the voltage signal depends heavily on the grid impedance value and will increase in the islanded mode of operation. As the grid impedance is usually low, these harmonics are relatively low and difficult to detect during normal operation. In the islanding operation mode, the grid impedance is replaced by the local load impedance, which can be much higher with respect to the grid impedance, so the harmonics population in the voltage will increase significantly and

can be used as valid indexes for islanding detection. Thus, the PSD coefficients of the voltage and current signals may be used as valid indexes for the islanding detection.

However, harmonic components in the signals occur in the case of some non-islanding events, such as external grid faults and component switching. The biggest challenge in designing islanding detection method here is how to differentiate these events, namely how to select appropriate threshold values for these parameters and assure not only islanding detection but to secure correct operation and avoid trip for non-islanding events too. Because of that, instead of predefined thresholds, SVM learning approach is utilized.

In this study, single phase voltage and current signals are measured with instrument transformers at PCC and their instantaneous values are processed to extract AR coefficients. These features are fed into the SVM models generated offline and islanding state is predicted, see Figure 12.

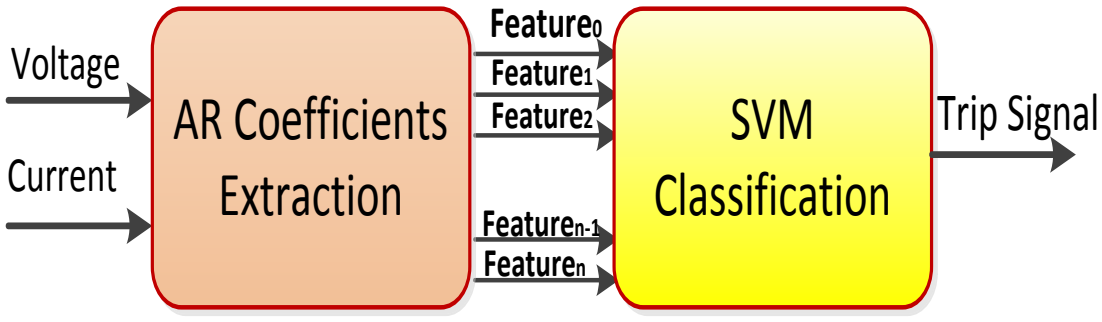


Figure 12 The Diagram of the Proposed Islanding Detection Technique

The proposed method shows great performances for the active power mismatch up to 40% and reactive power mismatch up to 5% while it may fail to detect islanding for the larger mismatches and therefore it is assumed that this method operates in parallel with OVR/UVR and OFR/UFR at the PCC. These relays should be set to detect islanding for more than 40% of active and 5% of reactive power mismatches which is high enough to avoid mis-operations due to external non-islanding events. OVR/UVR and OFR/UFR trip fast and accurate for islanding events with larger active and/or reactive power mismatches.

## 1.5 Organization of Dissertation

This dissertation is organized as follows. In the second section the literature review for the existing anti-islanding methods is presented. The third section gives the theoretical background for power system, signal processing and machine learning approaches used in this study. Details of the proposed algorithm solution, power system modeling, events simulation and data set generation are presented in the Section IV. The section V covers results and evaluation of the presented method. The study conclusions are summarized in Section VI.

# CHAPTER II

# CURRENT RESEARCH EFFORTS*

## 2.1 Introduction

So far, many anti-islanding methods have been proposed and these methods can be characterized as communication based and local measurement based methods. For the large scale DG integration, such as bulk wind plant integration, communication based methods known as transfer trip, are used. However, for the small DG units in the distribution system those methods are impractical due to cost of installation. Hence local measurement based methods that may be further classified into passive or active methods are used instead.

The local measurement based methods rely only on the system parameters measured at PCC and have their own advantages and disadvantages. The performance of the anti-islanding method is often defined by Non Detection Zone (NDZ) concept, see Figure 13. The NDZ represents the mismatch in active and reactive power generated by DG and dissipated by the local load for which the method will not be able to differentiate between islanding and normal operation [6].

---

* Part of the material in this section is reprinted from "Islanding Detection for Inverter-Based Distributed Generation Using Support Vector Machine Method," by Matic-Cuka B.and Kezunovic M., Smart Grid, IEEE Transactions on , vol.5, no.6, pp.2676,2686, Nov. 2014.doi: 10.1109/TSG.2014.2338736, with permission from IEEE, Copyright 2014.

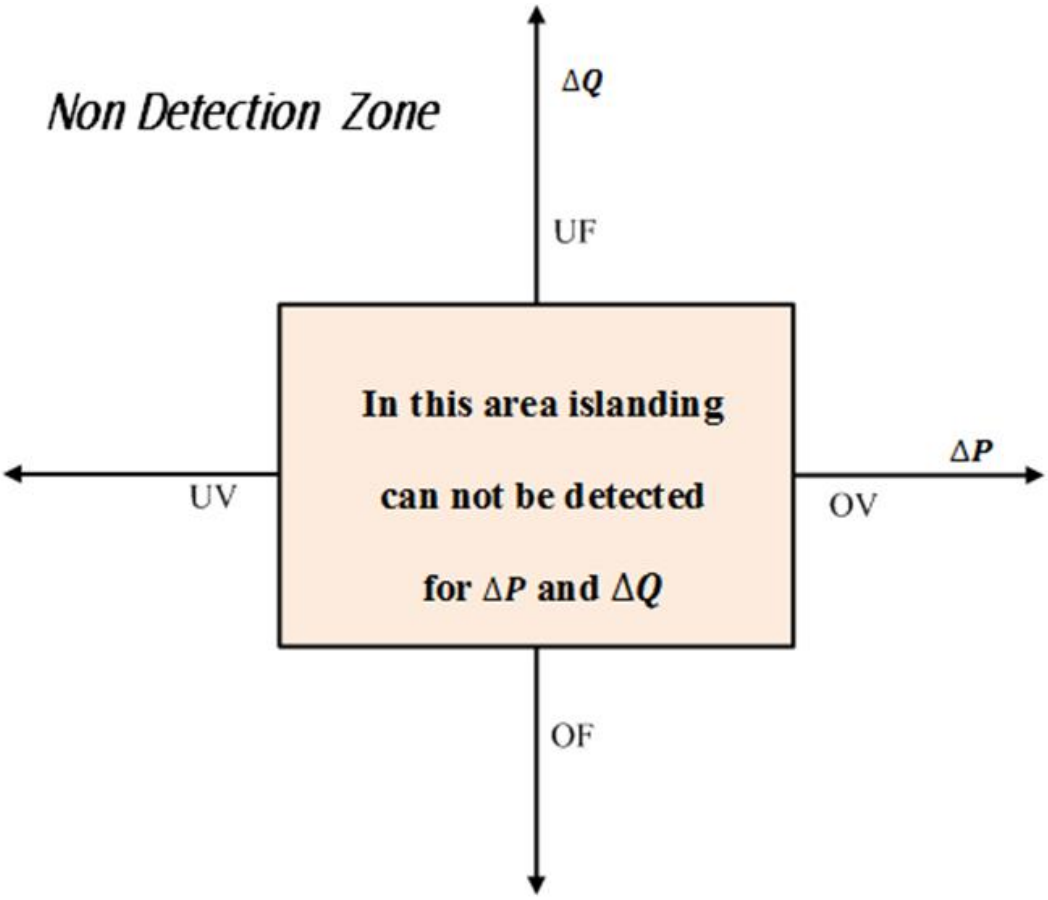


Figure 13 Non Detection Zone

## 2.2 Active Methods

The active methods are embedded into a control circuit of the power inverter and they are designed to inject small disturbances into the DG output. In the case of islanding those disturbances will cause system parameters to rise above the acceptable limits at PCC. This will trigger protective relays to disconnect a DG from the system.

The active frequency drift (AFD) [7], improved AFD [8], sandia frequency shift (SFS) [9], fuzzy SFS [10], automatic phase shift (APS) [11], sliding mode frequency shift (SMFS) [12], impedance measurement [13], singular and dual harmonic current injections [14,15], high frequency signal injection [16] output power variations [17], reactive power variation and control control [18,19] are examples of the active methods.

The active methods are categorized by small NDZ but they may deteriorate power quality during normal power system operation [20]. Besides, active methods may mis-operate in the system with multiple DGs due to mutual interference and cancelation of the injected disturbances [21] or they may have an effect on the system stability [22].

## 2.3 Passive Methods

On the other hand, the passive methods discriminate islanding from the normal condition based on the measurements of system parameters at the PCC. The signal parameter measurements or some features extracted from them are compared to the predefined thresholds.

The most common methods of this type are under/over voltage, under/over frequency [20], rate of change of frequency [23], phase jump detection [24], rate of change of frequency with power [25], rate of change of power with total harmonic distortion (THD) [26], voltage unbalance and total harmonic distortion of current signal [27], voltage and power factor change [26], energy mismatch for the harmonics [29] etc.

The passive methods do not have any negative impact on the grid operation, but they are characterized by larger NDZ than active methods. To decrease NDZ of the passive methods advanced signal processing tools such as Duffing oscillations [30] wavelet transform [31,32], S-Transform [32] have been utilized. However, these methods may be characterized by higher computational complexity and sensitivity to the noise.

In fact, the biggest challenges in designing the passive anti-islanding method are:

- How to select the right power system parameter(s) that will be monitored. There are vast of parameters that may be selected for monitoring at PCC. The parameters have to show unique characteristics that may be quantified for islanding and normal operating mode.
- How to select the right threshold values. These limits have to be low enough to detect islanding for small power generation/load mismatches and high enough to not operate for non-islanding events. Some grid transients have similar characteristics as islanding events and they may confuse anti-islanding protection at PCC to issue the trip signal.

Thus, the need still exists for the passive anti-islanding scheme that is effective in islanding detection and immune to the external non-islanding disturbances. Recently, it was recognized that learning from data is a useful way to analyze power system disturbances and in some cases it may be the most accurate method to extract the information and characterize some power system events [33]. The following chapter will

give description for several methods that uses machine learning methods to distinguish islanding condition.

### *2.3.1 Intelligent Islanding Detection Methods*

Unlike, active and passive islanding detection methods that depend on the determined threshold values, intelligent islanding detection methods relay on statistical and machine learning theories that extract signature characteristics of the event from the data set and use these knowledge to isolate an islanding condition on unseen data. According to [34,35,36] machine learning is an artificial intelligence concept that consists of training, or learning from data phase, and testing phase when it may generate output encoded in the same way as the target vectors.

### *2.3.2 A Bayesian Passive Islanding Detection Method*

Work in [37] proposes islanding detection for inverter based DG using Bayesian classifier. A statistical signal-processing algorithm known as estimation of signal parameters via rotational invariance (ESPRIT) techniques [33] is used to extract new features from measurements of the voltage and frequency at the PCC as islanding indicators. The features are defined based on a damped-sinusoid model for power system voltage and frequency waveforms, and include modal initial amplitudes, oscillation

frequencies, damping factors, and initial phases. The signal is modeled as a superposition of damped sinusoids in white noise as follows:

$$x(n) = \sum_{i=1}^{M} A_i e^{(\sigma_i + j\omega_i)n + j\phi_i} + z(n) \quad (2.1)$$

Where $A_i$ is the initial amplitude, $\sigma_i$ is the damping factor, $\omega_i$ is the frequency, $\phi_i$ is the initial phase, and $z(n)$ is the noise component in the signal, that is modeled as white noise.

Bayes' theorem states that

$$p(C = c|X = x) = \frac{p(X=x|C=c)p(C=c)}{p(X=x)} \quad (2.2)$$

In naïve-Bayes classifiers, X is a random variable indicating the feature, with being either a discrete value or a category, and is a random variable indicating the class of the record, with being the name of the class. This formula can be used to estimate the probability of a given test point belonging to class given its set of features.

The likelihoods are hence estimated as follows:

$$p(X = \{x_i\}|C = c) = \prod_i p(X_i = x_i|C = c) \quad (2.3)$$

This concept is well defined for categorical data. If is the total number of training points, is the number of training points belonging to class , and is the number of training points belonging to class and bin , likelihoods can be estimated as follows:

$$p(X \in m|C = c) = \frac{n_{cm}}{n_c} \quad (2.4)$$

$$p(C = c) = \frac{n_c}{n} \quad (2.5)$$

The authors obtained the waveforms for 600 events and ESPRIT was applied to each of the waveforms for feature extraction. There are 64 features extracted per

simulated event. These features are fed to a naïve-Bayes classifier that is modified to perform the three discretization methods. Three-fold cross-validation was used on the data, and each method was run for 10 iterations. The classification error is obtained and it is shown to be only 0.02%.

Thus, this method achieves high accuracy in islanding detection. However, due to high computational burden of running ESPRIT constantly on the new data windows this method may be used for verification purposes only. This scheme assumes knowledge of the islanding event's start time to initiate ESPRIT run and confirm islanding occurrence. Thus, this method cannot be used for islanding detection.

### *2.3.3 Decision Tree Approach*

Reference [38] uses decision tree approach to detect islanding condition. It utilizes and combines various system parameters as input features into the classifier. The decision tree approach is capable of breaking down a complex decision-making process into a set of simpler decisions, thus providing a solution that is often easier to interpret. The concept of this technique is based on recognizing the patterns of the sensitivities of some indices at a target location to prescribed credible events since every event could have a signature on the patterns of these indices. The behavioral model of the proposed islanding detection technique can be represented with in the decision tree as follows:

$$\underline{X} = \{X_1, X_2, \dots, X_n\}^T \tag{2.6}$$

$$X_i = \{x_{i_1}, x_{i_2}, \dots x_{i_j} \dots x_{i_m}\} \tag{2.7}$$

$$Y = \{y_1, y_2, \dots y_n\} \quad (2.8)$$

$$E = \{(X_k, y_k), k = 1,2, \dots, N\} \quad (2.9)$$

Where

$\underline{X}$ - dimensional vector denoting pattern (or classification) vector. It is called an ordered or numerical pattern if its independent variables take values from an ordered set, and categorical if its independent vectors take values from a set not having a natural ordering.

$X_i$ - pattern vector of the $X$; independent variables (or features) of the pattern vector $x_i$

$m$ - number of independent variables;

$Y$ -vector of class (or dependent) variables associated with $\underline{X}$

$y_1, y_2, \dots y_n$ class (or dependent) variables of the class vector $Y$

$(\underline{X}, Y)$ jointly distributed random variables with –dimensional vector denoting pattern vector and denoting the associated class vector of

$E$ vector of labeled credible events with a total number of $N$ events .

In this study, the following 11 indices are chosen and defined for any target distributed resource for $i^{th}$ event:

$x_{i_1} = \Delta f_i$ is frequency deviation in Hz.

$x_{i_2} = \Delta V_i$ is voltage deviation in pu.

$x_{i_3} = \left(\frac{\Delta f}{\Delta t}\right)_i$ is rate-of-change of frequency $\left(\frac{Hz}{s}\right)$

$x_{i_4} = \left(\frac{\Delta V}{\Delta t}\right)_i$ is rate-of-change of voltage $\left(\frac{pu}{s}\right)$

$x_{i_5} = \left(\frac{\Delta P}{\Delta t}\right)_i$ is rate-of-change of the power $\left(\frac{MW}{s}\right)$

$x_{i_6} = \left(\frac{\Delta f}{\Delta P}\right)_i$ is rate-of-change of frequency over power $\left(\frac{Hz}{MW}\right)$

$x_{i_7} = CTHD_i$ is total harmonic distortion of the current in pu

$x_{i_8} = VTHD_i$ is total harmonic distortion of the voltage in pu

$x_{i_9} = \Delta pf_i$ is power factor deviation

$x_{i_{10}} = (U\cos(\phi))_i$ is absolute value of the phase-voltage times power factor in pu

$x_{i_{10}} = (\frac{Ucos\phi}{\Delta t})_i$ is gradient of the of the voltage times power factor $\left(\frac{pu}{s}\right)$

This method uses a decision tree approach and it shows great robustness for the external grid events while it has 83.33% accuracy for islanding detection. Work in [39] applies adaptive boosting (AdaBoost) technique to improve decision tree accuracy. However, this approach is sensitive to outliners and the noisy data due to nature of the AdaBoost processing [40].

### *2.3.4 Decision Tree Classifier*

The decision tree classifier was utilized again in [41]. This method utilizes discrete wavelet transform to extract features from transient current and voltage signals. A decision-tree classifier uses the energy content in the wavelet coefficients to distinguish islanding events from other transient generating events. Discrete wavelet transform (DWT) was performed on the sampled waveforms with the Daubechie's 4 (Db4) mother wavelet. Then, the energy associated with DWT coefficients was obtained by integrating the square of the wavelet coefficient over a time window of 0.01 s.

The DWT of a sampled $f(k)$ signal is mathematically defined as:

$$DWT_{\psi}f(m,n) = \sum_k f(k)\psi^*_{m,n}(k) \quad (2.10)$$

Where mother wavelet is:

$$\psi_{m,n}(k) = \frac{1}{\sqrt{a_0^m}}\psi\left(\frac{k - nb_0a_0^m}{a_0^m}\right), \quad (2.11)$$

Where $a_0 > 0$ and $b_0 > 0$ are fixed real values, and are positive integers. The DWT analyzes a signal by decomposing the signal into a coarse approximation and detail information.

This method has a few drawbacks. First, the training data set used in the study has highly unbalanced class distribution. This phenomenon is well known in the machine learning theory and leads to overly optimistic results toward majority class [42]. Also, the signal sampling rate of 40 kHz used in the study is much higher than the typical 2-5 kHz sampling rate of the digital relays and recorders. Additionally, WT can not be used as a valid feature extraction tool for the signals in noisy environment. Thus, additional preprocessing is required.

### *2.3.5 Fuzzy Role Approach*

Work in [43] uses fuzzy role approach to detect islanding state. The proposed method develops a fuzzy rule-based classifier that was tested using features for islanding detection in distributed generation. In the developed technique, the initial classification boundaries are found out by using the decision tree (DT). From the DT classification boundaries, the fuzzy membership functions (MFs) are developed and the corresponding

rule base is formulated for islanding detection. But some of the fuzzy MFs are merged based upon similarity the measure for reducing the fuzzy MFs and simplifying the fuzzy rule base to make it more transparent. From the DT classification boundaries of the most significant features, trapezoidal fuzzy membership functions are developed and corresponding rule base is formed for classification. But some of the fuzzy MFs are merged depending upon the similarity measure and thus reducing the number of fuzzy MFs. From the reduced fuzzy MFs, a simplified fuzzy rule base is developed for islanding detection.

This work uses three features rate change of frequency, rate change of active power and voltage frequency deviation $\left(\frac{\Delta f}{\Delta t}, \frac{\Delta P}{\Delta t}, \Delta f\right)$ to develop the classification tree as shown in Figure 14.

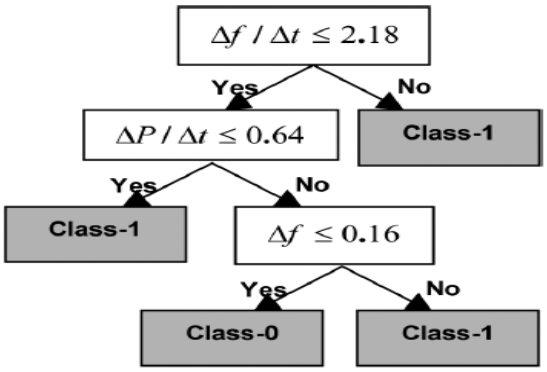


Figure 14 DT-based Islanding Detection (Class-1 Means Islanding and Class-0 means Non-islanding Condition) [43]

The most significant features, $\left(\frac{\Delta f}{\Delta t}, \frac{\Delta P}{\Delta t}, \Delta f\right)$, are considered as $X_1, X_2$ and $X_3$, respectively. Depending upon the values of the above three variables, the classification boundaries are decided for islanding detection. Thus, when $X_1$ is greater than 2.18, then the class is "1". If $X_1$ is less than 2.18 and $X_2$ less than 0.64, then the class "1". If $X_2$ is greater than 0.64 and $X_3$ less than 0.1664, then class "0", otherwise class "1". From the DT boundaries, trapezoidal MFs are developed for each variable, see Figure 15.

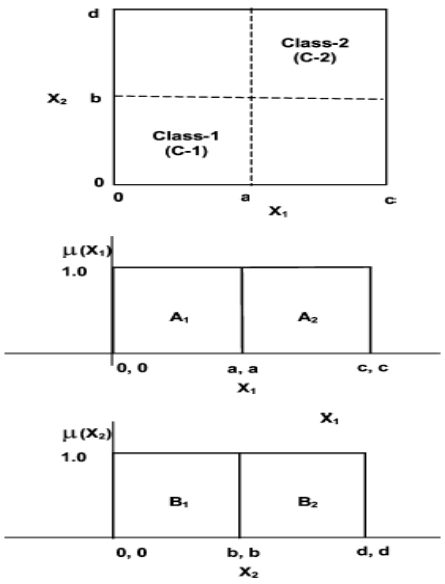


Figure 15 Decision Boundaries of the DT [43]

Depending upon the new fuzzy MFs, the rule base is simplified to:

$R_1$: If $X_1$ is $A_1$ and $X_2$ is W, then Class $-$ 1

$R_2$: If $X_1$ is $A_2$ and $X_2$ is $B_3$ , then Class $-$ 1

$R_3$: If $X_1$ is $A_2$ and $X_2$ is W and $X_3$ is $C_1$, then Class $-$ 1

$R_4$: If $X_1$ is $A_2$ and $X_2$ is $B_1$ and $X_3$ is $C_2$, then Class $-$ 0

This work uses a fuzzy role approach to detect islanding state and its performance shows great sensitivity to presence of the noise in the data set. Beside this method performances are dependent on the threshold setting on the decision tree split criterion.

### *2.3.6 Fuzzy Expert System Approach*

Reference [44] proposes method that uses fuzzy expert system approach. The following features are estimated for the target DG by passing the 3-phase voltage and current signals to the Fast Gauss-Newton algorithm FGNW algorithm:

$f_1 = \Delta f$ is frequency deviation in Hz

$f_2 = \left(\frac{\Delta f}{\Delta t}\right)$ is the rate of change of frequency in $\frac{Hz}{s}$

$f_3 = \left(\frac{\Delta V}{\Delta t}\right)$ is rate of change of voltage $\left(\frac{pu}{s}\right)$

$f_4 = \left(\frac{\Delta P_1^-}{\Delta t}\right)$ is the rate of change of negative sequence power $\left(\frac{MW}{s}\right)$

$f_5 = \left(\frac{\Delta P}{\Delta t}\right)$ is the rate of change of active power in $\left(\frac{MW}{s}\right)$

$f_6 = V_{ub,THD}$ is the total harmonic distortion of the voltage signal in pu

$f_7 = V_{ub,THD}$ is the total harmonic distortion of the current signal in pu

Similar to the approach presented in 2.3.1.4, a comparison between the classification values for the two classes and certainty factors is made using the various MFs. A fuzzy rule base is then derived, using the selected features for classification. The rules are framed as follows:

$R_{1:}$ If $F_2$ is $U_4$and $F_3$ is $U_5$ and $F_4$ is $U_{7,}$ then Class 1 with $CF_1$

$R_{2:}$ If $F_1$ is $U_2$and $F_2$ is $U_3$, then Class 1 with $CF_2$

$R_{3:}$ If $F_1$ is $U_1$and $F_4$ is $U_7$, then Class 1 with $CF_3$

$R_{4:}$ If $F_1$ is $U_2$and $F_3$ is $U_6$ and $F_4$ is $U_{8,}$ then Class 2 with $CF_4$

But if there are larger number of membership values in the firing strengths in previous equation and the fact that these values are always less than one, results in the classification values and also the certainty factors being lower than those obtained using the minimum t-norm.

$$CI = \max(\alpha_1 CF_1, \alpha_2 CF_2, \alpha_3 CF_3) \quad (2.12)$$

$$CNI = \alpha_4 CF_4 \quad (2.13)$$

The disadvantage of this method is that it requires complex calculation to obtain classifier input parameters.

## 2.4 Conclusion

In this chapter existing research efforts are presented. The benefits and disadvantage of each method type are described. Active methods are characterized by small NDZ, but they may have adverse effects on power system operation. On the other

hand, passive methods do not interfere with power system operation, but they are characterized by larger NDZ and may have high computational burden. Thus, based on the literature review lack of the islanding method that is reliable, easy to implement, does not have adverse effect on the power system operation and has low computational burden still remains.

CHAPTER III

THEORETICAL BACKGROUND

## 3.1. Introduction

To design and evaluate performances of an algorithm that utilizes machine learning principle, following steps should be considered: input parameters selection, features extraction and classification, see Figure 16.

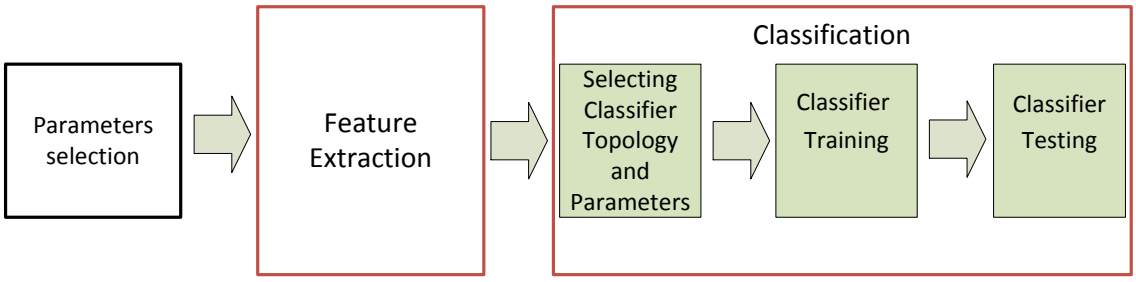


Figure 16 Classification System

To perform input parameter selection effect of the event of interest, in this case islanding on the power system parameters should be analyzed. In the case of islanding, many power system parameters such as frequency, active power, reactive power, and voltage, current and different combinations of these parameters and their characteristics in time and frequency domain are available. In this study, the voltage and current

parameters have been selected as input parameters due to changes in their frequency content for the case of the islanding mode of operation.

In the second step, the feature extraction from the input parameters should be performed. The extracted features from the signals should be uncorrelated and able to characterize and differentiate power system events of the interest. This step is very important to achieve successful event classification. For some applications waveform measurements data may be used as input to the classifier and since these data do not require any processing, this step may be omitted. However majority of applications require some form of the data processing. Tues, the features extracted from the signals are used as the inputs to a classification system instead of the signal waveform itself because it may lead to reduction in the input feature vector dimension and increase in the speed of classification process.

Today there are many signal processing methods that can be chosen as candidates for feature extraction and calculation of the signal features and each is characterized by different performance and complexity. Generally, all signal-processing methods may be categorized into two classes:

- transform-based methods
- model-based methods.

Transform based methods may decompose measurements into time domain or frequency domain components. The advantage of this type of signal processing method is that they do not require any prior knowledge about the measured signal. The most

often used filter based methods are a variation of the Fourier transforms (FFT) and the Wavelet transform.

On the other hand, model-based methods depend on the prior knowledge of system and assume that the data sequences are generated from certain models. Some examples of the model-based methods are:

- sinusoidal models methods:
    - estimation of signal parameters via rotational invariance techniques (ESPRIT)
    - multiple signal classification (MUSIC)
- autoregressive model methods:
    - autoregressive moving-average (ARMA)
    - autoregressive (AR)
    - moving-average (MA)
- state space models
    - Kalman Filters

One of the advantages of model-based methods is that if the model is correctly chosen, it can achieve a high-frequency resolution as compared with transform-based methods. Conversely, if an incorrect model is applied, the performance is rather poor. In this study AR signal modeling is used to extract signal features.

In the third step, the classifier topology and proper classifier parameters have to be selected. The classification models have to be obtained in the training phase and its performances should be evaluated on the test data set. Again, there are many different

classifiers available today, such as neural networks (NN), multilayer perceptrons (MPC), Baysine classifier, SVM etc. and each has its own distinct characteristics. In this research, SVM was chosen.

SVM is based on statistical learning theory [45] and the input space is nonlinearly mapped onto a high-dimensional feature space using kernels. The result is that the classes are more likely to be linearly separable than in a low-dimensional feature space. SVM is based on the Structural Risk Minimization theory that minimizes an upper bound on the expected risk and minimizes the generalization error. More details about SVM may be found in Section 3.3.

In this study, voltage and current signals at PCC are used as input parameters and (AR) signal modeling is applied to extract feature vectors form voltage and current signals while Support vector Machine (SVM) is selected as a classifier. The theoretical background of power systems, signal processing and machine learning approaches are presented in the following sections.

## 3.2. Parameter Selection Problem

The Figure 17 shows an equivalent circuit for the inverter based DG system. In this simplified circuit the DG inverter is modeled as a voltage source operating with multiple frequencies which depend on the employed pulse width modulation technique. The LCL filter ($R1$, $L1$, $R2$, $L2$, $R3$ and $C3$) has been modeled considering ideal passive elements and the non-intentional islanding operation is simulated by means of the switch

*sw*. Similar like in [46], the dependency of $V_{PCC}$ and $I_{PCC}$ from $V_{DG}$ in normal mode of operation and islanding mode of operation can be analyzed as:

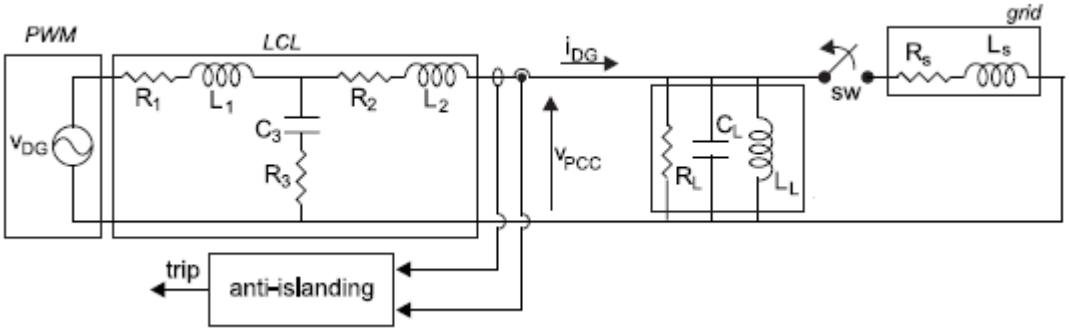


Figure 17 Equivalent Circuit of Inverter Based DG System

$$Z_1(j\omega) = j\omega L_1 \tag{3.1}$$

$$Z_2(j\omega) = j\omega L_2 \tag{3.2}$$

$$Z_3(j\omega) = R_3 + \frac{1}{j\omega C_3} \tag{3.3}$$

$$Z_L(j\omega) = R_L || \frac{1}{j\omega C_L} || j\omega L_L \tag{3.4}$$

$$Z_G(j\omega) = R_G + j\omega L_G \tag{3.5}$$

$$V_{PCC}(j\omega) = V_{DG}(j\omega) \frac{Z_3(j\omega)(Z_L(j\omega)||Z_G(j\omega))}{Z_1(j\omega)Z_2(j\omega)+Z_1(j\omega)Z_3(j\omega)+Z_2(j\omega)Z_3(j\omega)+(Z_1(j\omega)+Z_3(j\omega))Z_L(j\omega)||Z_G(j\omega)} \tag{3.6}$$

$$I_{PCC}(j\omega) = \frac{V_{PCC}(j\omega)}{Z_L(j\omega)||Z_G(j\omega)} \tag{3.7}$$

Dependency of $V_{PCC}$ and $I_{PCC}$ from the $V_{DG}$at different frequency component different than fundamental may be evaluated as:

$$\left|\frac{\partial V_{PCC}}{\partial V_{DG}}\right| = \left|\frac{Z_3(j\omega)(Z_L(j\omega)||Z_G(j\omega))}{Z_1(j\omega)Z_2(j\omega)+Z_1(j\omega)Z_3(j\omega)+Z_2(j\omega)Z_3(j\omega)+(Z_1(j\omega)+Z_3(j\omega))Z_L(j\omega)||Z_G(j\omega)}\right| \quad (3.8)$$

$$\left|\frac{\partial I_{PCC}}{\partial V_{DG}}\right| = \left|\frac{1}{Z_L(j\omega)||Z_G(j\omega)}\right| \left|\frac{\partial V_{PCC}}{\partial V_{DG}}\right| \quad (3.9)$$

In order to comply with the IEEE Standard 1457 requirements, the effect of high frequency components of the DG system on voltage and current signals at PCC have to be minimized. Thus the parameters$Z_1$, $Z_2$ and $Z_3$ for LCL filter have to be chosen carefully.

For the case of islanding mode of operation, switch opens and the equations (3.8)-(3.9) become:

$$\left|\frac{\partial V_{PCC}}{\partial V_{DG}}\right|_{island} = \left|\frac{Z_3(j\omega)Z_L(j\omega)}{Z_1(j\omega)Z_2(j\omega)+Z_1(j\omega)Z_3(j\omega)+Z_2(j\omega)Z_3(j\omega)+(Z_1(j\omega)+Z_3(j\omega))Z_L(j\omega)}\right| \quad (3.10)$$

$$\left|\frac{\partial I_{PCC}}{\partial V_{DG}}\right|_{island} = \left|\frac{1}{Z_L(j\omega)}\right| \left|\frac{\partial V_{PCC}}{\partial V_{DG}}\right| \quad (3.11)$$

According to the (3.8)-(3.11) the variation into frequency spectrum for $V_{PCC}$ and $I_{PCC}$ may be used as parameters for islanding detection.

### 3.3. Autoregressive Signal Modeling

This section describes the basic theory for parametric modeling of signals using AR method. AR method is model-based method of spectral estimation and it is assumed that signal satisfy generating model with known functional form and thus the parameters of the model can be estimated. The spectral characteristics are than divided from the

estimated model. To do so, the model order or the structure has to be selected too. There are several methods available for model order selection, such as Akaike Information Criterion (AIC) [47], Generalized Information Criterion (GIC) [48], Bayesian Information Criterion (BIC) [49], etc.

First, the relation between power spectral density (PSD) of the input and output of a linear system has to be analyzed, see Figure 18.

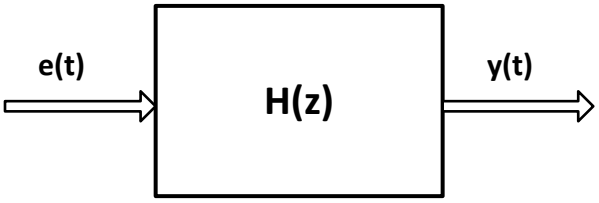


Figure 18 PSD of the Input and Output for the Linear System

The stable linear time-invariant system is defined as:

$$H(z) = \sum_{k=-\infty}^{\infty} h_k z^{-k} \tag{3.12}$$

The symbol $z^{-1}$ denotes unity delayed operator defined by $z^{-1}y(t) = y(t-1)$. Also let $e(t)$ be the input and $y(t)$ output of the system. Then, they are related by the convolution sum

$$y(t) = H(z)e(t) = \sum_{k=-\infty}^{\infty} h_k e(t-k) \tag{3.13}$$

Thus the transfer function of this filter is

$$H(\omega) = \sum_{k=-\infty}^{\infty} h_k e^{-i\omega k} \tag{3.14}$$

Covariance function of the $y(t)$ is defined as

$$r(k) = E\{y(t)y^*(t-k)\} \tag{3.15}$$

The symbol * is used to denote complex conjugate of the scalar variable.

Thus from (3.14) and (3.15) we obtain

$$r_y(k) = \sum_{p=-\infty}^{\infty} \sum_{m=-\infty}^{\infty} h_p h_m^* E\{e(t-p)e^*(t-(m+k)\}$$

$$= \sum_{p=-\infty}^{\infty} \sum_{m=-\infty}^{\infty} h_p h_m^* r_e(m+k-p) \tag{3.16}$$

The Power Spectral Density PSD is defined as DTFT of the covariance sequence:

$$\phi(\omega) = \sum_{k=-\infty}^{\infty} r(k) e^{-i\omega k} \tag{3.17}$$

Thus by inserting (3.16) into (3.17) we get relationship between PSD of the input and output of the stable and time-invariant linear system.

$$\phi_y(\omega) = \sum_{k=-\infty}^{\infty} \sum_{p=-\infty}^{\infty} \sum_{m=-\infty}^{\infty} h_p h_m^* r_e(m+k-p) e^{-i\omega(k+m-p)} e^{i\omega m} e^{i\omega p}$$

$$= \sum_{p=-\infty}^{\infty} h_p e^{-i\omega p} \sum_{m=-\infty}^{\infty} h_m^* e^{i\omega m} \sum_{\tau=-\infty}^{\infty} r_e(\tau) e^{-i\omega\tau}$$

$$= |H(\omega)|^2 \phi_e(\omega) \tag{3.18}$$

A rational spectra is a rational function of $e^{-i\omega}$:

$$\phi(\omega) = \frac{\sum_{k=-m}^{m} \gamma_k e^{-i\omega k}}{\sum_{k=-n}^{n} \rho_k e^{-i\omega k}} \tag{3.19}$$

Where $\gamma_{-k} = \gamma_k^*$ and $\rho_{-k} = \rho_k^*$.

According to Weierstrass approximation theorem [50] any continues PSD can be closely approximated a rational PSD of the form (3.19) if degrees $m$ and $n$ are chosen sufficiently large. Thus the rational PSD will form a dense set in the class of all continuous spectra.

Since $\phi(\omega) \geq 0$ the rational spectral density in (3.19) may be written as

$$\phi(\omega) = \left|\frac{B(\omega)}{A(\omega)}\right|^2 \sigma^2 \tag{3.20}$$

Where $\sigma^2$ is positive scalar and $A(\omega)$ and $B(\omega)$ are polynomials:

$$A(\omega) = 1 + a_1 e^{-i\omega} + \cdots + a_n e^{-in\omega} \tag{3.21}$$

$$B(\omega) = 1 + b_1 e^{-i\omega} + \cdots + b_m e^{-im\omega} \tag{3.22}$$

The equation (3.19) can be expressed in Z-domain:

$$\phi(z) = \frac{\sum_{k=-m}^{m} \gamma_k z^{-k}}{\sum_{k=-n}^{n} \rho_k z^{-k}} \tag{3.23}$$

Than

$$\phi(z) = \sigma^2 \frac{B(z)B^*(\frac{1}{z^*})}{A(z)A^*(\frac{1}{z^*})} \tag{3.24}$$

We may note that zeroes and poles of (3.24) are symmetric pars about the unit circle and if we assume that (3.24) has no poles with modules equal to one than the region of convergence for $\phi(z)$ is unity circle$z = e^{i\omega}$.

From (3.18) and (3.20) it may be concluded that the rational PSD spectra from (3.20) can be associated with a signal obtained by filtering white noise of power $\sigma^2$ through rational filter with transfer function $H(\omega) = \left|\frac{B(\omega)}{A(\omega)}\right|$.

The fact that 3.19 can be written as 2.24 is called spectral factorization theorem and it means that parameterized model of $\phi(\omega)$. Thus the spectral estimation problem is turned into problem of signal modeling. Estimating the frequency spectrum of $x(t)$ thus becomes estimating the model parameters $a_i$ under a selected criterion.

The signal that satisfies

$$y(t) = \frac{B(z)}{A(z)} e(t) \tag{3.25}$$

Depending on the model order selection the signal may be called:

- autoregressive moving average signal, $ARMA\ (n, m)$, for $m > 0, n > 0$
- autoregressove signal, AR(n), for $m = 0, n > 0$
- moving average signal, MA, for $m > 0, n = 0$.

In this study we are focused on AR signal model and expressions for coeficients model calculation is provided next.

By using AR approach the signal is represented as the response of a linear time invariant system with white noise as input, where system is modeled by finite number of poles. In a $AR(p)$ model, the data sample at time $t$ is defined by the following equation:

$$y(t) = -\sum_{i=1}^{p} a_i y(t-i) + b_0 e(t) \tag{3.26}$$

where $a_i$ represents AR coefficients, $e(t)$ is white Gaussian noise, $b_0$ stands for noise variance.

First, we multiply (3.26) with $y^*(t-k)$ and taking expectation yields to

$$r(k) + \sum_{i=1}^{p} a_i r(k-i) = b_0 E\{e(t) y^*(t-k)\}, \ \ k > 0 \tag{3.37}$$

We can write transfer function as

$$H(z) = \frac{B(z)}{A(z)} = \sum_{k=0}^{\infty} h_k z^{-k}, \quad h_0 = 1 \tag{3.38}$$

It gives $y(t) = H(z)e(t) = \sum_{k=0}^{\infty} h_k e(t-k)$ (3.39)

$$E\{e(t)x^*(t-k)\} = E\{e(t) \sum_{s=0}^{\infty} h_s^* e^*(t-k-s)\} = \sigma^2 h_{-k}^* \tag{3.40}$$

For $h_k = 0, k < 0 \ \ r(k) + \sum_{i=1}^{p} a_i r(k-i) = b_0 \sigma^2 h_{-k}^*\}$ (3.41)

since $h_s = 0$ for $s < 0$.

$$r(k) + \sum_{i=1}^{p} a_i r(k-i) = 0, \;\; k \geq 0 \tag{3.42}$$

The covariance expression of the AR process may be used to estimate $a_i, \; i = 1 \ldots p$ parameters by replacing the true autocovariance function $r(k) = E\{x(t)x(t-k)\}$ with estimates obtained from data [51]. The covariance can be written as

$$r(k) + \sum_{i=1}^{p} a_i r(k-i) = 0, \;\; k > 0 \tag{3.42}$$

and

$$r(0) + \sum_{i=1}^{p} a_i r(-i) = {b_0}^2, \;\; k = 0 \tag{3.44}$$

From (3.42) and (3.43) for $k = 1, \ldots, p$ Yule-Walker or normal equations are obtained:

$$\begin{bmatrix} r(0) & r(-1) & \ldots & r(-p) \\ r(1) & r(0) & \ldots & r(1-p) \\ & & \ldots & \\ & & \ldots & \\ r(p) & r(p-1) & \ldots & r(0) \end{bmatrix} \begin{bmatrix} 1 \\ a_1 \\ . \\ . \\ a_p \end{bmatrix} = \begin{bmatrix} {b_0}^2 \\ 0 \\ . \\ . \\ 0 \end{bmatrix} \tag{3.45}$$

If $r\{(k)\}_{k=0}^{p}$ were known we could solve (3.45) for

$$\theta = \left[a_{1,\ldots,a_p}\right]^T \tag{3.46}$$

by using all but the first row. Once θ is obtained, ${b_0}^2$ can be found easily from (2.24). We can write equation for the order p as following:

$$R_{p+1}\begin{bmatrix}1\\ \theta_p\end{bmatrix}=\begin{bmatrix}{b_0}^2\\ 0\end{bmatrix} \tag{3.47}$$

In order to reduce the number of flops to calculate $\{\theta_p, {b_0}^2\}$ the order recursive solution called Levinson-Durbin algorithm [51] is used.

The AR parametric modeling has found broad applications in analysis of biomedical signals [52] and recently has been discovered as a powerful tool for power system disturbances analysis, such as low frequency oscillations estimation [53] and fault detection and location [54].

The AR model gives inherent data compression without loss of essential information and smooth frequency spectrum can be obtained from AR coefficients, while maintaining all important signal features. The Figure 19 aligns spectrums obtained using FFF and AR of the voltage signal at PCC for the 0% active and reactive power mismatch.

## 3.4. Support Vector Machine

SVM tool has become a popular tool for power systems analysis, such as load or device type identification in an electrical system [55, 56], power system transient stability assessment [57], and distance relay blocking and blackout mitigation [58]. In this study it is used for islanding detection.

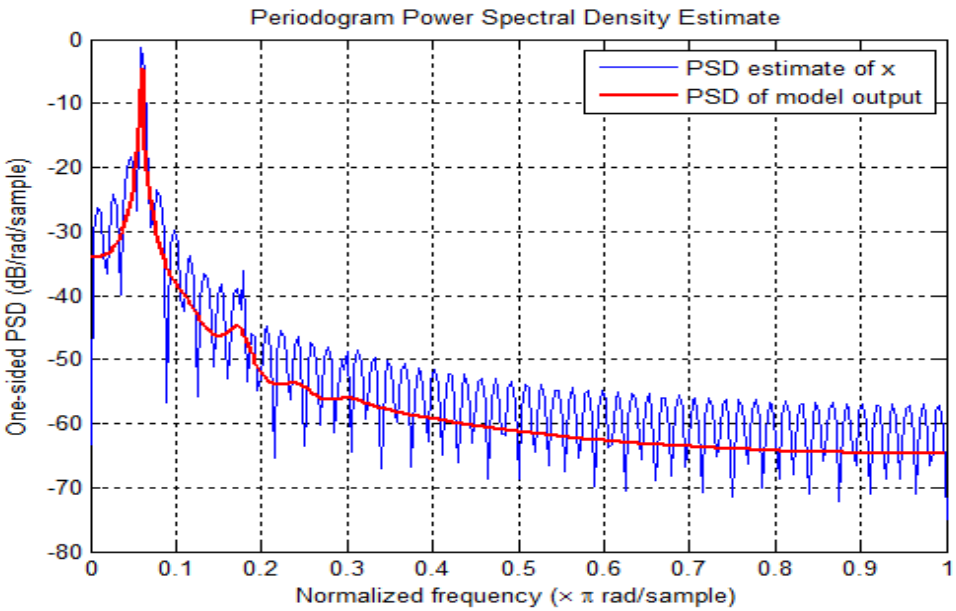


Figure 19. Periodogram vs. AR PSD Estimation of the Voltage Signal at PCC for the 0% Active and Reactive Power Mismatch

This section describes the basic theory for Support vector Machine (SVM) algorithm. The SVM is based on statistical learning theory and it is used for binary classification problems. The main idea behind SVM is to map the input feature vectors into a very high dimensional feature space through some nonlinear mapping that is chosen a priori. The result is that the classes are more likely to be linearly separable than in a low-dimensional feature space. To do so optimal hyperpline in this space which separates multidimensional data into two classes has to be constructed. The aim of the SVM classifier is to produce mapping function in the training phase that will predict the class label in the testing phase where only feature attributes are used as inputs . A special characteristic in designing a SVM is that, instead of the dimension reduction commonly

employed in conventional pattern recognition systems, the input space in a SVM is nonlinearly mapped onto a high-dimensional feature space.

Given a training set of $l$ instance and label pairs $(x_i, y_i)$ $i = 1 \dots l$, where each example has $d$ inputs $x_i \in R^d$ and class label with one of two values $y_i \in \{1, -1\}^l$, That is, each object can belong to one out of two classes.

First, we apply a nonlinear function $\phi(\cdot)$ that maps the input space $R^d$ onto a high-dimensional feature space $\mathbb{F}$,

$$\phi: R^d \rightarrow \mathbb{F}, x_i \rightarrow \phi(x_i) \tag{3.48}$$

Once a high-dimensional feature space $\mathbb{F}$ is chosen, another function $f(\cdot)$ is applied to map the feature space onto a decision space, see Figure 20,

$$f: \mathbb{F} \rightarrow Y, \quad \phi(x_i) \rightarrow \mathbb{F}(\phi(x_i)) \tag{3.49}$$

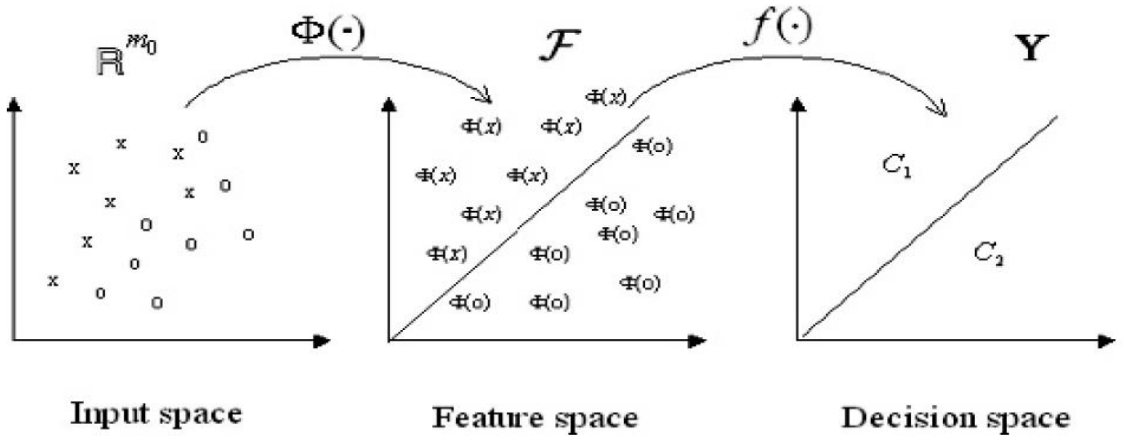


Figure 20 Different Spaces and Mappings in SVM [33]

All hyperpline in Ƒ may be parametrized by vector $w$ and a constant, expressed in

$$w \cdot \phi(x_i) + b = 0 \tag{3.50}$$

Where $w$ is a vector orthogonal to the hyperplane. Given hiperplane $(w, b)$ that separates the data, this gives the function

$$f\big(\phi(x_i)\big) = sign(w \cdot \phi(x_i) + b) \tag{3.51}$$

Which correctly classifies the training data, and hopefully classifies unseen or testing data as well. However, a given hyperplane represented by $(w, b)$ is equally expressed by all pairs $\{\lambda w, \lambda b\}$ for $\lambda \in R^+$. So we de_ne the canonical hyperplane to be that which separates the data from the hyperplane by a distance of at least1 1. That is, we consider those that satisfy:

$$w \cdot \phi(x_i) + b \geq 1 \text{ when } \quad y_i \geq 1 \tag{3.52}$$

$$w \cdot \phi(x_i) + b < 1 \text{ when } \quad y_i < 1 \tag{3.53}$$

Or

$$y_i(w \cdot \phi(x_i) + b) \geq 1, \forall i \tag{3.54}$$

All such hyperlines have a functional distance greater than 1. To obtain geometric distance from the hyperplane to the data point (3.54) has to be normalized by the magnitude of $w$:

$$d((w, b), x_i) = \frac{y_i(w \cdot \phi(x_i) + b)}{\|w\|} \geq \frac{1}{\|w\|} \tag{3.54}$$

The goal is to maximize geometric distance to the closest data point. From the equation (3.54) we may see that magnitude $\|w\|$ has to be maximized. To do so the Lagrange multiplayer is used. The problem is transferred into optimization problem:

$$\text{Minimize: } W(\alpha) = -\sum_{i=1}^{l} \alpha_i + \frac{1}{2}\sum_{i=1}^{l}\sum_{j=1}^{l} y_i y_j \alpha_i\, \alpha_j (\phi(x_i), \phi(x_j))$$

$$\text{Subject to } \sum_{i=1}^{l} y_i \alpha_i = 0 \;\; , \;\; 0 \le \alpha \le C, \;\; \forall i \tag{3.54}$$

Where $\alpha$ is the vector of $l$ non negative Lagrange multiplayers to be determined and C is a constant.

It was seen that the optimal hyperline can be written as linear combination of the training examples.

$$w = \sum_i \alpha_i\, y_i\, \phi(x_i) \tag{3.55}$$

It can be shown that

$$\alpha_i (y_i (w \cdot \phi(x_i) + b) - 1) \ge 0, \quad \forall i \tag{3.56}$$

Which means that only the closest data points contribute to $w$, because when the functional distance of data point is greater that 1 then $\alpha_i = 0$.

The training examples for which $\alpha_i > 0$ are called support vectors and they are the only one needed in defining optimal hyperplane.

If we insert (3.51) into (3.55):

$$f(x) = sign([\sum_i \alpha_i\, y_i\, \phi(x_i)] \cdot \phi(x_i) + b)$$

$$= sign(\sum_i \alpha_i\, y_i\, (\phi(x_i) \cdot \phi(x_i)) + b) \tag{3.57}$$

Thus, if we know the formula (called Kernel) for the dot product in the higher dimensional feature space

$$K(x_a, x_b) = \phi(x_a) \cdot \phi(x_b) \tag{3.58}$$

We do not need to deal with the mapping to the future space directly. Thus, a kernel function which is a function dependent only on the difference from the test set and the support vectors from the training set is used to nonlinearly project the input space onto a high-dimensional feature space, see Figure 21.

Despite many kernels being proposed by researchers, see Table II, in this work Radial Bias Function (RBF)

$$K(x_i, x_j) = e^{-\gamma\|x_i - x_j\|^2}, \gamma > 0 \tag{3.59}$$

kernel for soft margin C-SVM is used. C and $\gamma$ can be determined experimentally through the use of a cross-validation process.

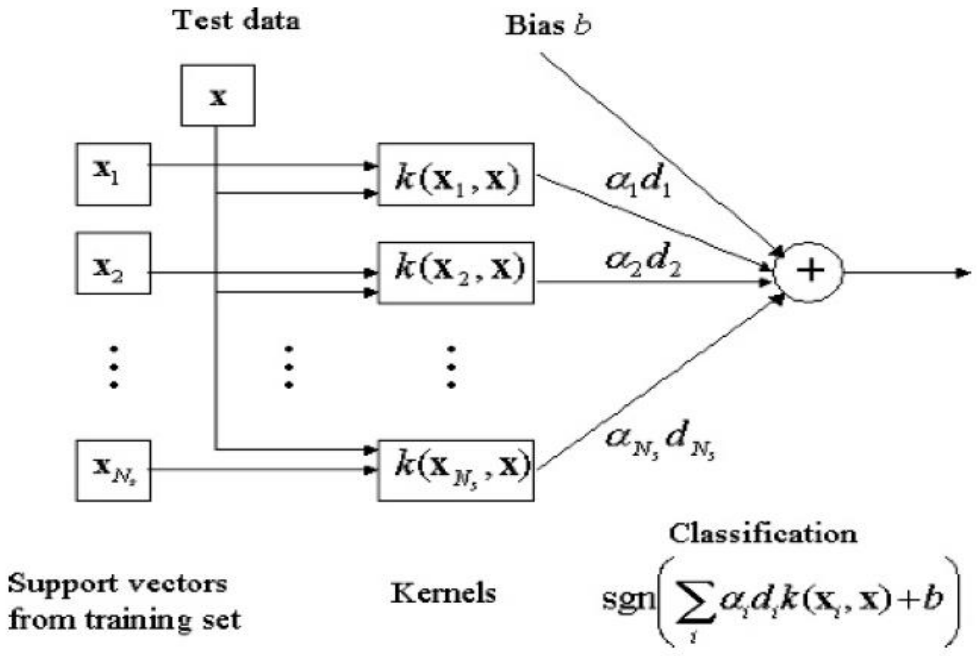


Figure 21 Block Diagram of SVM Classifier for Two Class Case [33]

As one usually does not know in advance which parameters are the best for a given application, these parameters must be determined during the machine learning. A commonly used procedure is to apply cross-validation [33]. A k-fold cross-validation can be described as follows: For a given training set, one first divides the data set into k subsets of equal size. The classifier is then trained k times: In the l^th iteration, l = 1, 2, . . . ,k, the classifier is trained using all subsets except the l^th subset. The trained classifier is then tested using the l^th subset, and the classification error for this subset is then computed. In such a way, each training subset is tested once and the cross-

Table II SVM Kernels

| | |
|---|---|
| Polynomial | $k(x,y) = (\langle x,y\rangle + \theta)^d$ |
| Gaussian RBF | $k(x,y) = e^{(\frac{-\|x-y\|^2}{\gamma})}$ |
| Exponential RBF | $k(x,y) = e^{(\frac{-\|x-y\|}{\gamma})}$ |
| Sigmoidal | $k(x,y) = \tanh(\langle x,y\rangle + \theta)$ |
| Inverse multiquadratic | $k(x,y) = \frac{1}{\sqrt{\|x-y\|^2 + \gamma^2}}$ |
| B-spline | $k(x,y) = B_{2N+1}(\|x-y\|)$ |
| Additive kernel | $k(x,y) = \sum_i k_i(x,y)$ |
| Tensor product of kernels | $k(x,y) = \prod_i k_i(x,y)$ |

validation accuracy is the percentage of data which are correctly classified. Finally the average of these errors is taken as the expected prediction error.

## 3.5. Conclusion

In this chapter, theoretical background for the proposed method is presented. It is shown that frequency content of voltage and current signals change during islanding condition and that these features may be used as parameters to differentiate islanding mode of operation. The process of AR molding and parameter calculation form the signal is presented. The fundamental principle of SVM is shown as well. The concepts of hyperplane, generalization error, kernel, cross-validation, etc are defined.

# CHAPTER IV

# PROPOSED ISLANDING DETECTION METHOD*

## 4.1. Introduction

In this chapter new approach of islanding detection for single phase inverter based DG is presented [59]. The concept of proposed method and validation procedure are described at the beginning. Then, the details of the power system used in the study and data set generation and simulations are reviewed.

## 4.2. Anti-islanding Scheme Description

The steps in designing and validation of the proposed SVM-based anti-islanding protection scheme are presented in Figure 22. Single phase voltage and current signals are selected as input parameters for the proposed method. The instantaneous values of these signals are obtained in multiple PSCAD/EMTDC simulations and data set consisting of 700 events is generated. Afterwards signals representing each event are processed using Yule-Walker method to calculate AR coefficients and noise variance. The signal window of 50ms and AR model order $p$=30 are used for the AR coefficients

* Part of the material in this section is reprinted from "Islanding Detection for Inverter-Based Distributed Generation Using Support Vector Machine Method," by Matic-Cuka B.and Kezunovic M., Smart Grid, IEEE Transactions on , vol.5, no.6, pp.2676,2686, Nov. 2014.doi: 10.1109/TSG.2014.2338736, with permission from IEEE, Copyright 2014.

calculations. The model order is selected using common rule that AR order should be around one third of the data window size. The result of processing are two sets of AR coefficients, one corresponding to voltage and second corresponding to current signal. The voltage and current signals are decomposed into 31 parameters (30 AR coefficients and noise variance) each. Thus, for every simulation run, 62 feature parameters (31 parameters of the current and 31 parameters of the voltage current signals) and a class label that describes operation mode of the system ("1" for islanding and "-1" for non-islanding) are stored as a single database entry.

The feature normalization assures that each feature in the feature vector is unbiased and properly scaled so that different features are equally weighted in a classifier since there is no a priori information on which feature is more important than the others. The process of feature normalization is applied as:

$$\dot{x}_i = \frac{x_i - \mu_i}{\sigma_i}, \; i = 1 \ldots k \tag{4.1}$$

where:

$k$- feature dimension

$\sigma_i$- standard deviation of the $i$th feature

$\mu_i$-mean value of the $i$th feature

To estimate SVM model parameters and to evaluate performance of the selected model on the unseen data set the 5-fold cross validation and bootstrap method [60] are used, respectively. The bootstrapping is a general statistics technique that iterates the computation of the algorithm accuracy on a resampled dataset. The Bootstrap iterator

will generate a user defined number of independent training and testing data set splits to check whether proposed data model is biased to the training and testing data set.

The Radial Bias Function (RBF) kernel is used in this study. This kernel requires two parameters to be selected: the regularization parameter $C_p$ and kernel parameter $\gamma$. The values of the both parameters C and γ are varied in the range from $2^{-5}$ to $2^{10}$ and $2^{8}$ to $2^{-8}$, respectively. For the any parameter combination 5-fold cross-validation is performed. The data set is split in 5 parts, where 4 parts are used to train and 1 part to test, the parts are rotated so that error is evaluated evenly across all examples. The values C=8 and γ=0.0625 are shown to be the best combination for the proposed application. This process is repeated for 10 replications, until the error rate converges, with different training and test splits. The average detection accuracy computed in this way is a good estimator of the SVM model generalization accuracy.

### 4.3. Power System Description

In order to demonstrate proposed concept, a study case using IEEE 13-bus test system is used. The single phase inverter-based DG and local load are connected to the node 692, see Figure 23. The simulations are carried using PSCAD/EMTDC [61] simulation tool. The sampling frequency used in the study is 2 kHz.

The main objective of power electronic inverter is to supply high quality power output to utility grid. The power inverter should be able to convert dc current power to ac power and obtain synchronization with the grid. Depending on the size of the DG

system, power inverters could have single phase or three phase structure [62]. The PV systems used in the roof top residential units have single phase topology while large size PV and wind systems used in power plants have three phase topology. In this study, single phase inverter topology is utilized.

The structure of the single phase inverter-based DG is presented in Figure 24. Additionally, the local load, filter topology, transformer and the point where measurement for current and voltage signals are recorded are illustrated too.

The DG system parameters are listed in Table III. The low-pass filter, with the parameters in Table II is employed as interface between inverter and the grid to reduce the effect of inverter's current harmonics to comply with IEEE 1547. The DG is connected to the distribution system through a single phase 0.12/4.16kV transformer. The decoupled current control interface presented in [15] is used in the study.

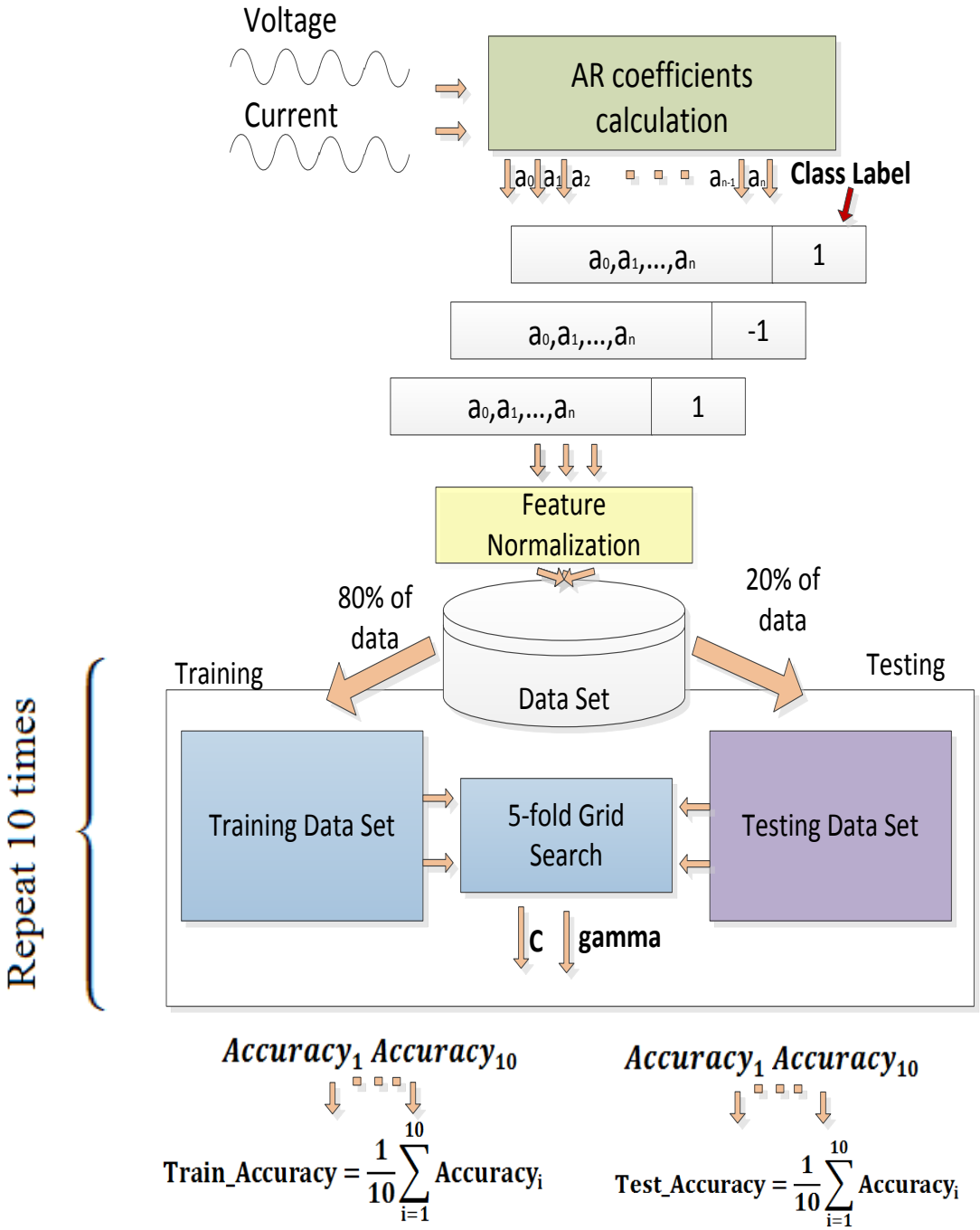


Figure 22 Anti-islanding Scheme Design and Validation

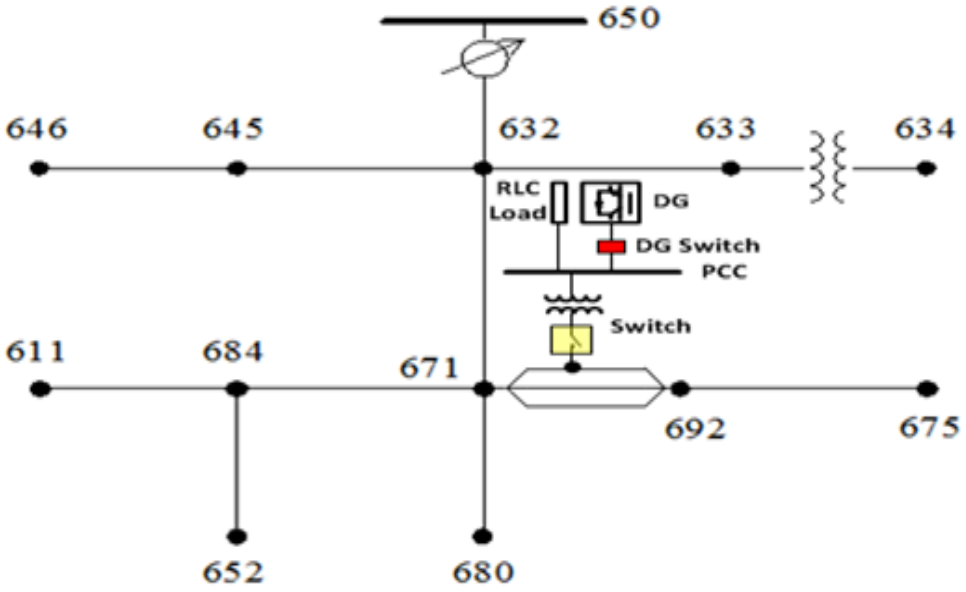


Figure 23. Diagram of the IEEE 13 Distribution Test System [41]

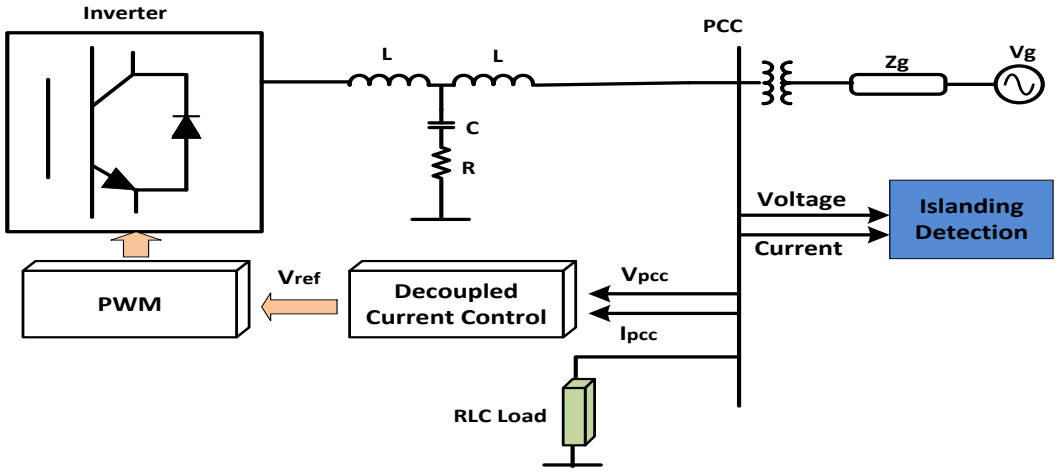


Figure 24 DG System Used in the Study

Table III DG System Parameters

| **Parameter** | **Value** |
|---|---|
| **Voltage** | 120 V |
| **DG Output Power** | 5kW |
| **Switching Frequency** | 8kHz |
| **Input DC Voltage** | 400 V |
| **Filter Resistance (R)** | 1 Ω |
| **Filter Inductance (L)** | 3 mH |
| **Filter Capacitance (C)** | 12μF |

Figure 25 shows decoupled current control topology. Measurements of the PCC voltage are fed to a phase-locked loop (PLL) that extracts the frequency and phase information from the signal. Park's transformation is then applied on the DG output current to obtain the dq components. After comparison with the set points of the currents, the error signals are passed to proportional-integral (PI) controllers. The output is amplified, and then used together with the frequency to generate the sinusoidal signal needed by the pulse-width modulator (PWM) that controls the inverter-based DG switches. With the control topology described, DG conditioning system is capable of supplying sinusoidal waveform current into utility grid.

In compliance with the IEEE Standard 1547 , the real power output is maintained constant to minimize current and voltage harmonic distortion at the point of

interconnection and the reactive power output is regulated to zero to achieve near unity power factor.

To investigate effects of the multiple DGs interaction on the classifier performances, the second invertor-based DG with the same control interface and parameters is added to a phase A of the node 675.

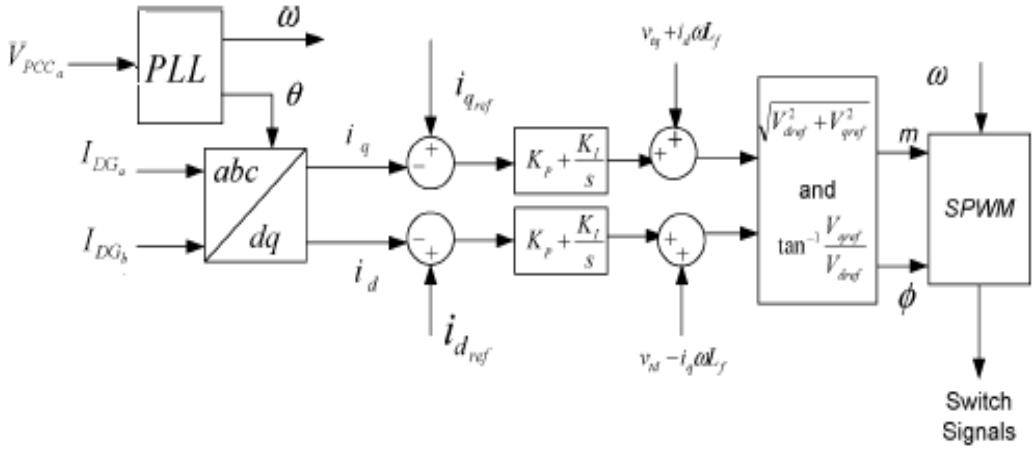


Figure 25. A Block Diagram of Closed Loop Synchronous Frame Current Control [15]

### 4.4. Data Set Generation

According to IEEE 1457, see Figure 26 the islanding method should be tested with the local load for various mismatches of active and reactive power. The test conditions require that an adjustable RLC local load should be connected in parallel between the DG inverter and the grid.

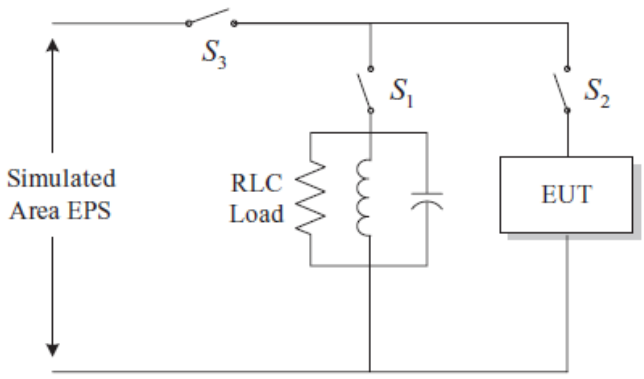


NOTES
1 – Switch $S_1$ may be replaced with individual switches on each of the RLC load components
2 – Unless the EUT has a unity output p.f., the receiver power component of the EUT is considered to be a part of the islanding load circuit in the figure .

Figure 26 Test Set up for the Anti-islanding Requirements in IEEE 1547[3]

The IEEE 1457 anti-islanding testing requirements may be summarized as:

- The active and reactive power mismatch between active/reactive power generated by DG and active/reactive power dissipated by the local load should be set to zero, $\Delta P = 0, \Delta Q = 0$.
- Resonant frequency of the local load should be adjusted to be the same as the frequency of the power grid this means that local load does not dissipate any reactive power.

$$f_r = \frac{1}{2\pi\sqrt{LC}} = 60\ Hz \tag{4.2}$$

- One more load parameter called quality factor is defined. The quality factor is energy stored vs. energy dissipated by the local load per circle:

$$Q_f = R\sqrt{\frac{C}{L}} \tag{4.3}$$

The reactive power generated by *C* [VAR] should equal the reactive power absorbed by *L* [VAR] and should equal the power dissipated in *R* [W] at the nominal power *P* and rated grid voltage *V*. To comply with the IEEE Standard 1547 the quality factor of the load should be set to 1.During the islanding mode of operation, local load with high quality factor has very low impedance and behaves as law pass filter. Because of that, signal harmonics content change at PCC is negligible.

Thus the parameters for the local RLC load can be calculated as

$$R = \frac{V^2}{P} \tag{4.4}$$

$$L = \frac{V^2}{2\pi f P Q_f} \tag{4.5}$$

$$C = \frac{PQ_f}{2\pi f V^2} \tag{4.6}$$

Under these conditions and for the case of the islanding mode of operation the DG and the local load will continue to resonate at the grid frequency and rated voltage. Here the changes in the voltage and frequency parameters are insignificant to detect the islanding condition. Because of this it is necessary to develop more sophisticated methods that are able to detect the islanding for the small power mismatches.

To develop efficient anti-islanding protection method and to quantify its performances, the external grid transients have to be taken into consideration too. Besides analyzing method's performances of islanding detection for different active/reactive power mismatches, equally is important to test method's sensitivity for

the fault and grid component switching. For these grid transients the voltage and current signals at PCC may behave similarly as for the case of islanding events. Tues, robustness of the proposed method for the external non islanding events has to be taken into consideration in designing and testing new method.

The DG system is connected to the distribution system and various non-islanding grid events that may have similar system response as islanding are simulated too. To test algorithm performances for grid transients IEEE 13 distribution feeder system is used. The same single phase switch is used to create all islanding events.

In this study, the authors carefully constructed the data set to cover wide range of events. We simulated islanding events modeling local load as constant RLC. We did not consider nonlinear load type, because for the most islanding detection methods, RLC load type is the most difficult to be detected [20]. Also, we simulated non-islanding events to evaluate the robustness of the method, such as grid faults and switching transients. We varied event parameter, location and loading conditions. More details about the test generation follow.

In order to test the proposed method, 700 training cases were generated. Islanding cases were generated for active power mismatches up to 40% of the rated power of the DG and varying the reactive power mismatches up to 5% of the DG rating.

The following process is used to select optimal data set:

a. The arbitrary data set is generated and model parameters and prediction accuracy are estimated.

b. Then, additional data points are added to the data set and the parameter tuning and accuracy are then estimated again.
c. After several steps of adding additional data to the data set and performing calculation, results for both classifier parameters and accuracy will converge. That means that the optimal data set size is reached.

The fact that method accuracy converged on the 700 data set proves method's performances. A case where method's performance drastically changes every time new data is added refers that classifier is unstable. This means that either the classifier cannot be applied for that problem or more data has to be generated for the data set.

The feature vectors represent AR coefficients for voltage and current signals calculated using 50 ms data window captured immediately after transient occurrence. The data set is generated in such a way that the number of islanding (positive) and non-islanding (negative) events is evenly balanced. There are 350 non-islanding and 350 islanding events. Non-even spread of the positive and negative events may lead to biased detection of one category of the events.

The set of 350 islanding cases is generated for different combinations of the active and reactive power mismatches. An adjustable RLC load is connected in parallel between the DG inverter and the grid and islanding conditions are simulated by opening the single phase switch, Figure 26. The mismatch power generated by DG and dissipated by the load is varied up to 40% for active and 5% for reactive power.

The set of 350 non-islanding cases is generated by applying faults at different locations in the grid and by switching static loads, motor loads, and capacitor banks at

different points in the system as well as switching second DG at node 675. The single, double and three phase faults whose resistance and duration are varied are simulated. The resistance is changed from 1Ω to 5Ω and duration is set as 2ms, 4ms and permanent faults. The islanding and non- islanding events are simulated for light system loading conditions up to 40 % of the base load maintaining the constant load power factor.

The more details about case generation may be found in Table IV.

Table IV Generated Data Set

| **Cases** | **No. of Data Samples** | **Description** |
|---|---|---|
| **Islanding** | 300 | ±40 % active power and ±5% reactive power mismatch |
| **Non-islanding** | 25 | Load Switching |
| **Non-islanding** | 25 | Capacitor Switching |
| **Non-islanding** | 25 | Motor Load Switching |
| **Non-islanding** | 225 | Faults |
| **Islanding** | 25 | Light load; various power mismatches |
| **Non-islanding** | 25 | Faults at different locations |
| **Islanding** | 25 | While Second DG is connected |
| **Non islanding** | 25 | Second DG Switching |

## 4.5. Conclusion

In this section detail description of the proposed method is given. AR coefficients that model PSD function are used as input parameters for new anti-islanding scheme. Due to complexity of the problem and impact of grid transients on the signals at PCC, fixed threshold limits will not be applicable here. Instead, SVM classifier is applied to discriminate islanding condition from the AR coefficients for voltage and current signals at PCC. The process of selecting right classifier parameters and algorithm validation are shown. Beside this, the power system and simulations details used in the study are presented as well.

# CHAPTER V

# RESULTS AND EVALUATION*

## 5.1. Introduction

In this chapter the performances of the proposed method are evaluated. At the beginning the feature vectors extraction in the form of AR coefficients of voltage and current signals is presented. Then, classification accuracy is obtained for each event type followed by the overall accuracy of the algorithm. Impact of the data window length on the algorithm accuracy and implementation details are provided at the end.

## 5.2. Feature Extraction

The main purpose of this section is to present AR modeling as feature extraction tool. Events presented in this section cause minimal deviation in the system parameters and are among the most challenging to detect.

Figure 27 shows the system response of the voltage and current signals at PCC of an islanding event for zero active/reactive power mismatches. For this event, DG and the

---

* Part of the material in this section is reprinted from "Islanding Detection for Inverter-Based Distributed Generation Using Support Vector Machine Method," by Matic-Cuka B.and Kezunovic M., Smart Grid, IEEE Transactions on , vol.5, no.6, pp.2676,2686, Nov. 2014.doi: 10.1109/TSG.2014.2338736, with permission from IEEE, Copyright 2014.

local load are resonating at system frequency and nominal voltage value. Tues the voltage and current magnitudes do no change for this case.

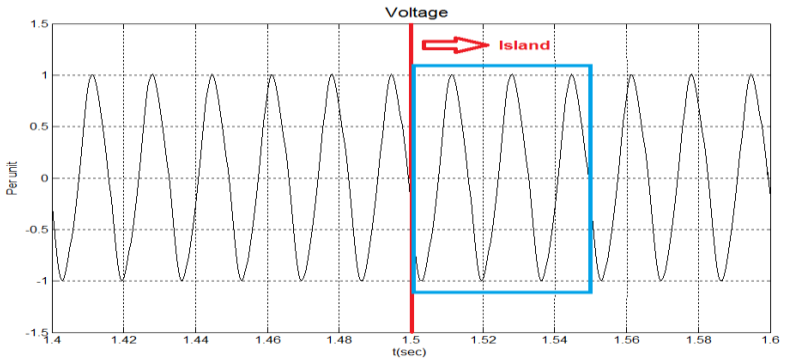


(a.)

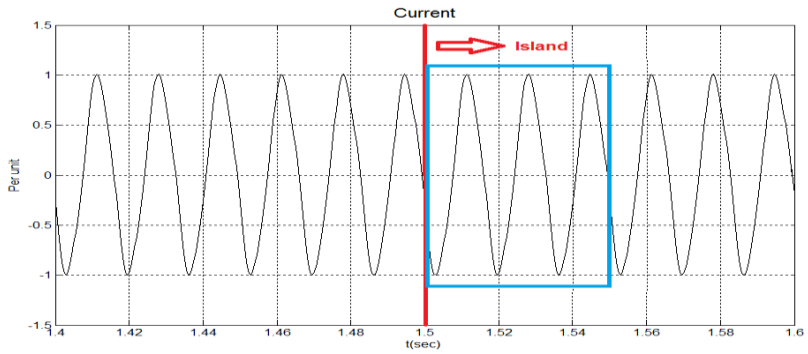


(b)

Figure 27 (a) PCC Voltage and (b) PCC Current for an Islanding Event for Zero Active/Reactive Power Mismatch

The Figures 28-30 show grid fault, capacitor switching and load switching events, respectively. For the load switching, the magnitude of the voltage increases 3% while for the capacitor switching and grid fault events voltage magnitudes decrease 2%

and 5%, respectively. On the other hand, the current magnitudes change in such a way to maintain constant real power output.

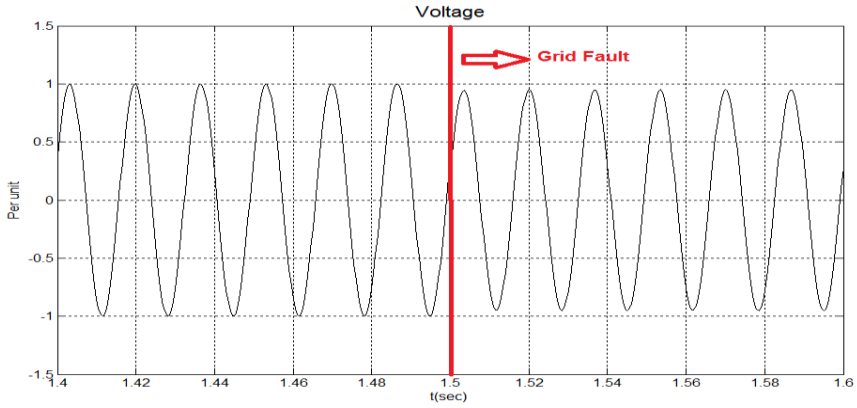


(a)

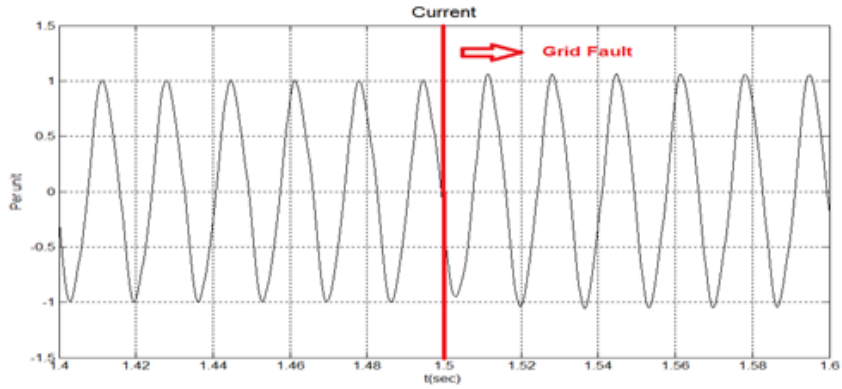


(b)

Figure 28 (a) PCC Voltage and (b) PCC Current for A-phase Grid Fault Event at Bus 675.

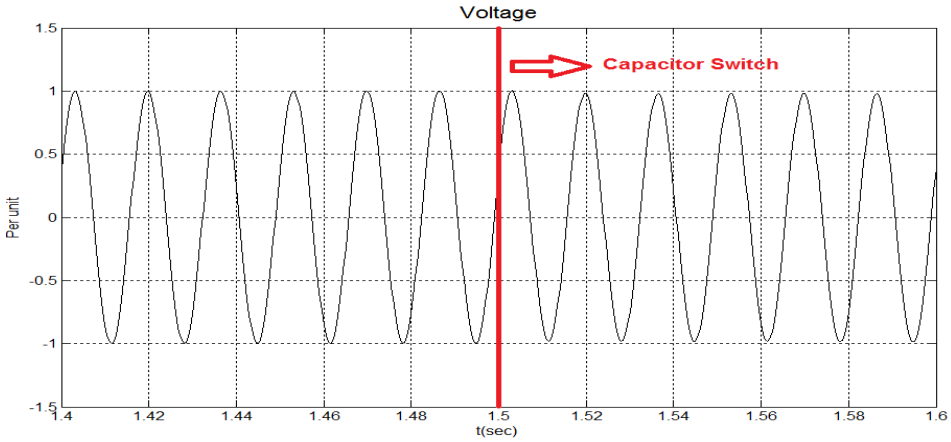


(a)

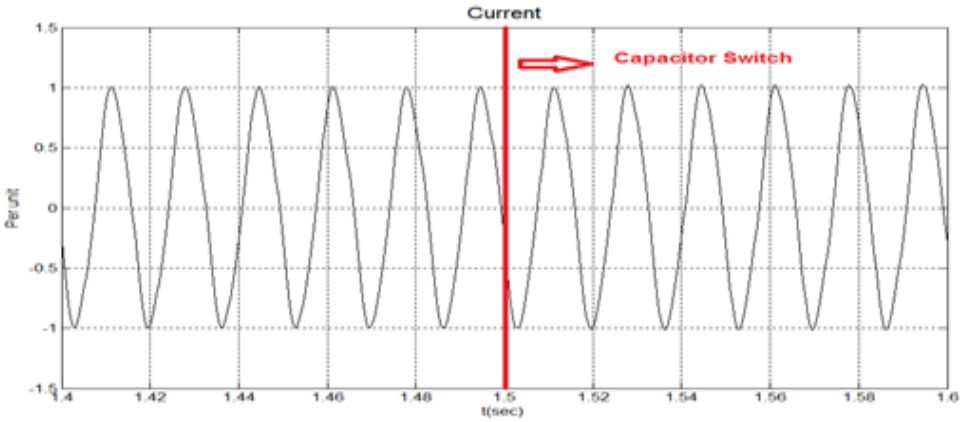


(b)

Figure 29 (a) PCC Voltage and (b) PCC Current for Capacitor Switching Event at Bus 692

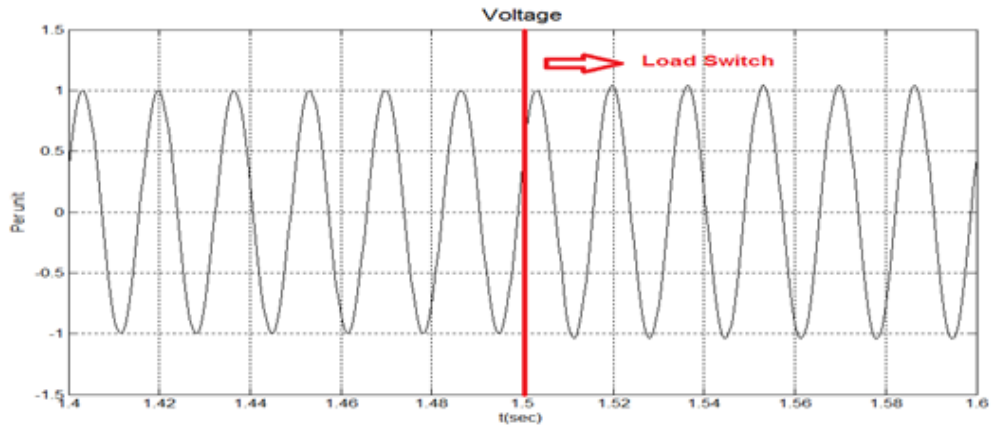


(a)

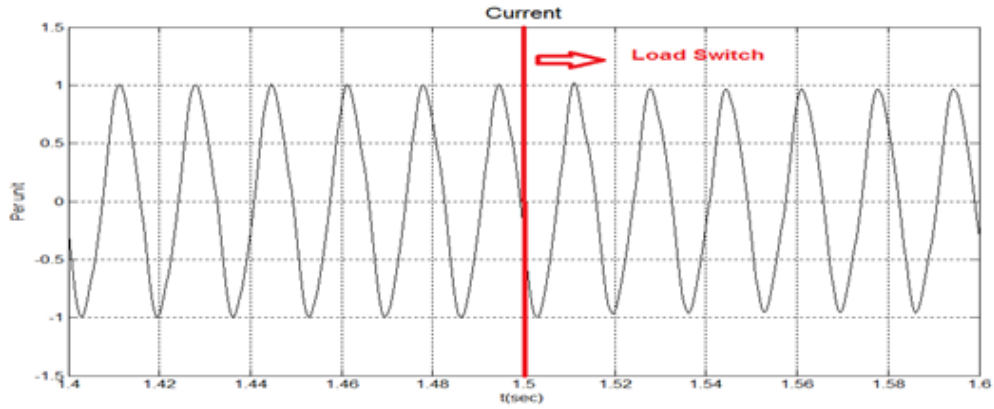


(b)

Figure 30 (a) PCC voltage and (b) PCC current for load switching event at bus 675

The 50 ms data window is used to calculate noise variance and AR coefficients for the voltage and current signals for the events from Figure 27-30. The AR coefficients for voltage signals are shown in Figure 31 and AR coefficients for current signals are shown in Figure 32.

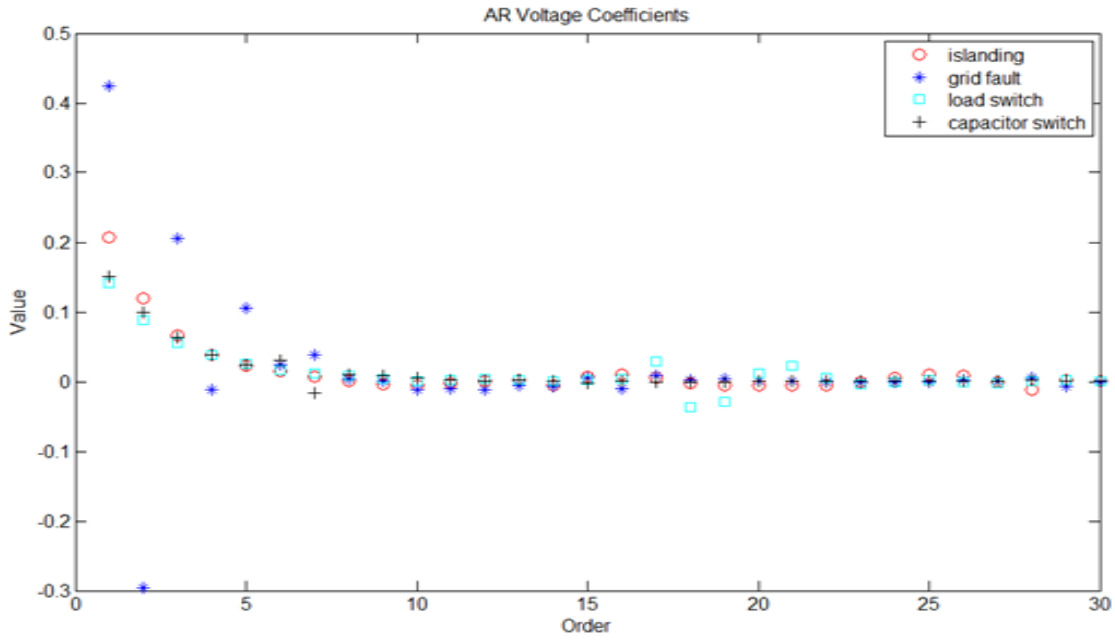


Figure 31 AR Coefficients of the Voltage Signal at PCC for Islanding, Fault, Load Switching and Capacitor Switching Events

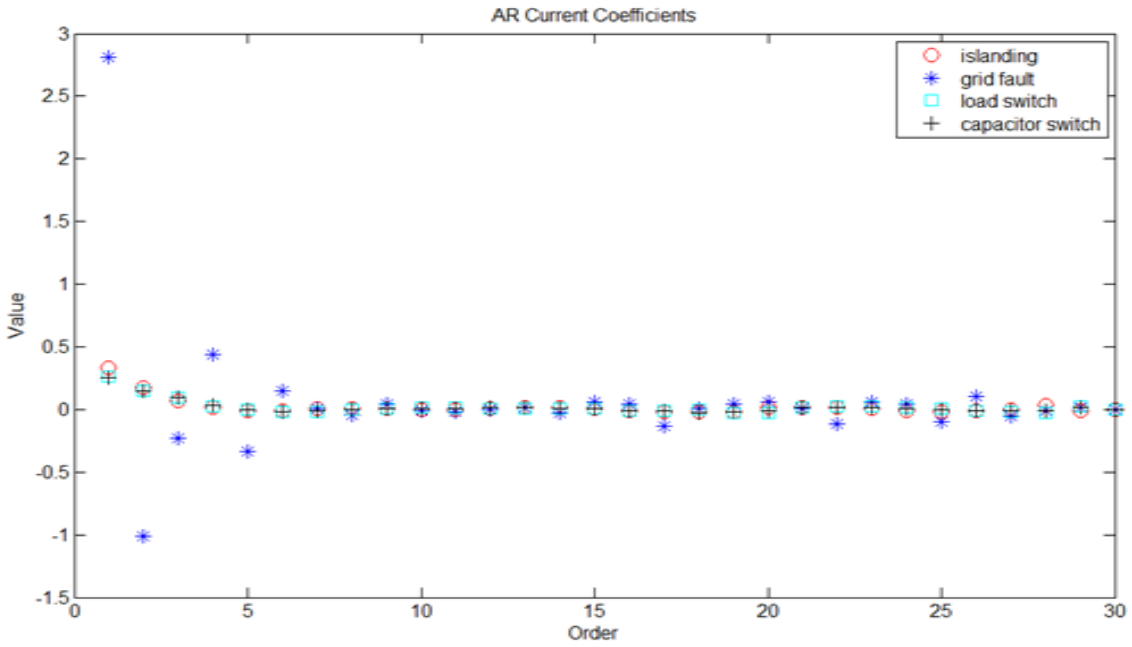


Figure 32 AR Coefficients of the Current Signal at PCC for Islanding, Fault, Load Switching and Capacitor Switching Events

Figure 33-37 show AR coefficients from multiple simulations per event type.

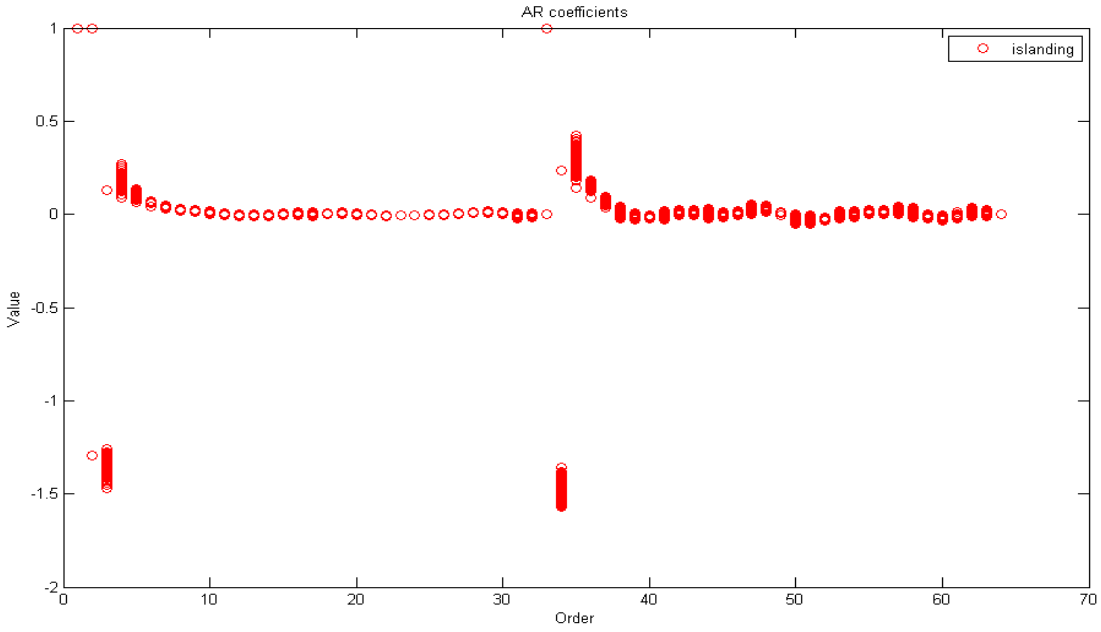


Figure 33 AR Coefficients of the Voltage and Current Signals at PCC for Islanding Events

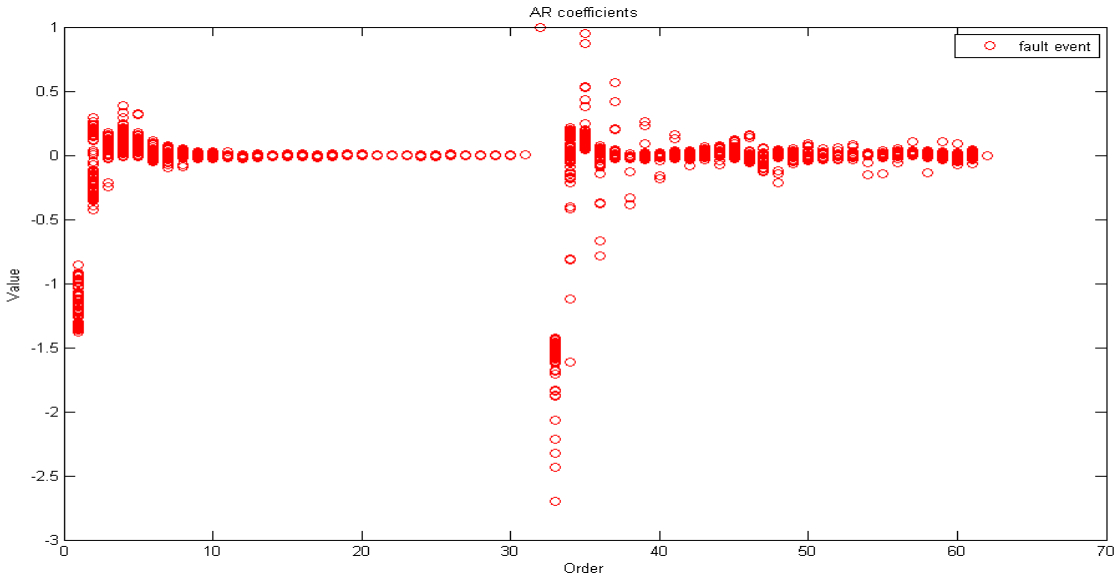


Figure 34 AR Coefficients of the Voltage and Current Signals at PCC for Grid Fault Events

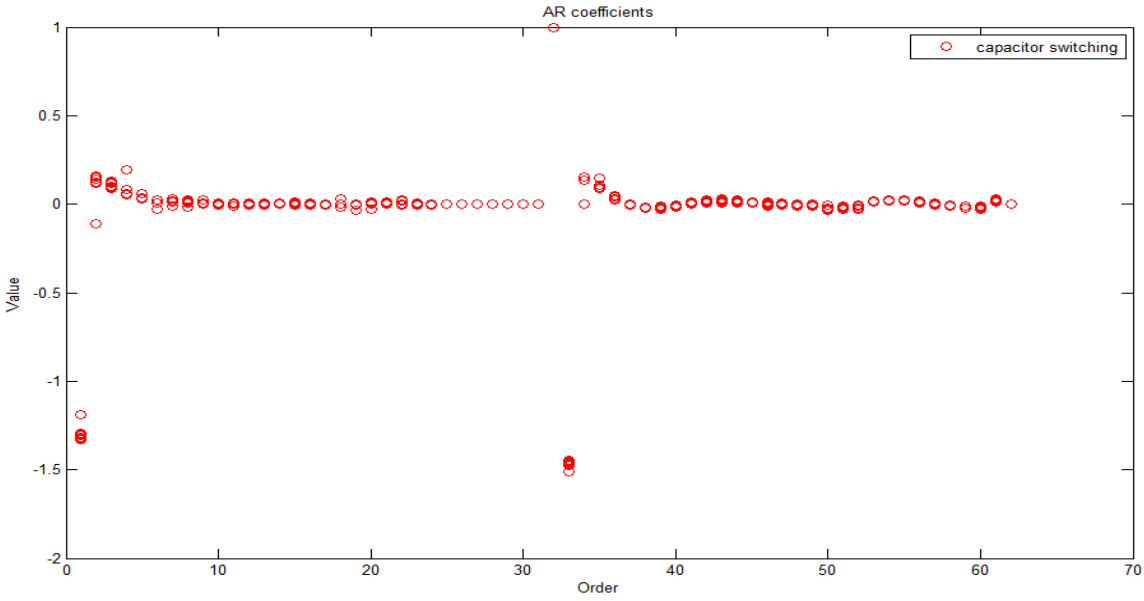


Figure 35 AR Coefficients of the Voltage and Current Signals at PCC for Capacitor Switching Events

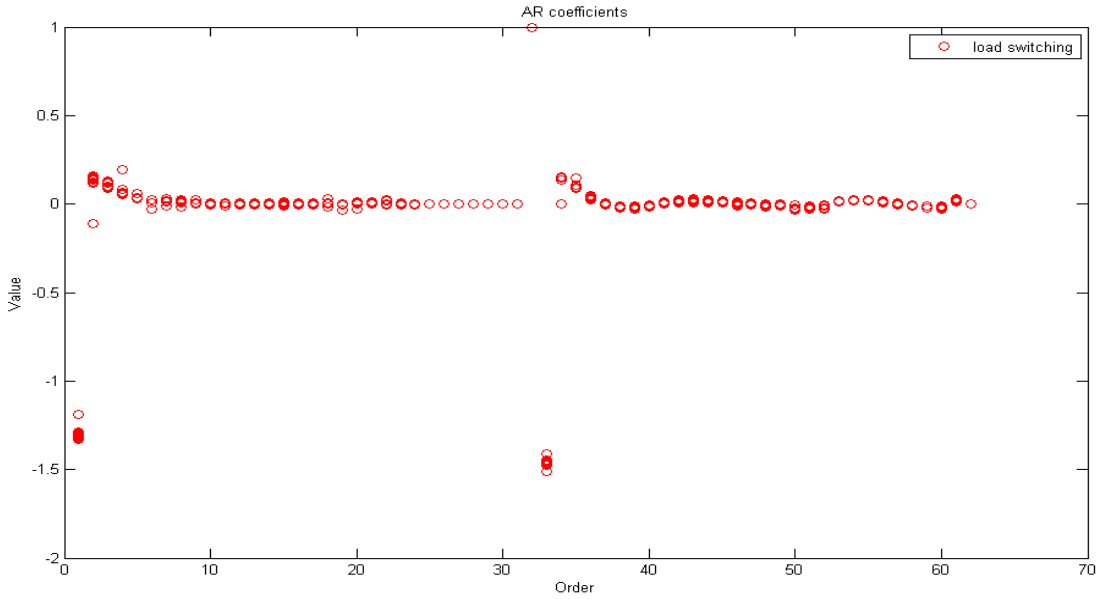


Figure 36 AR Coefficients of the Voltage and Current Signals at PCC for Load Switching Events

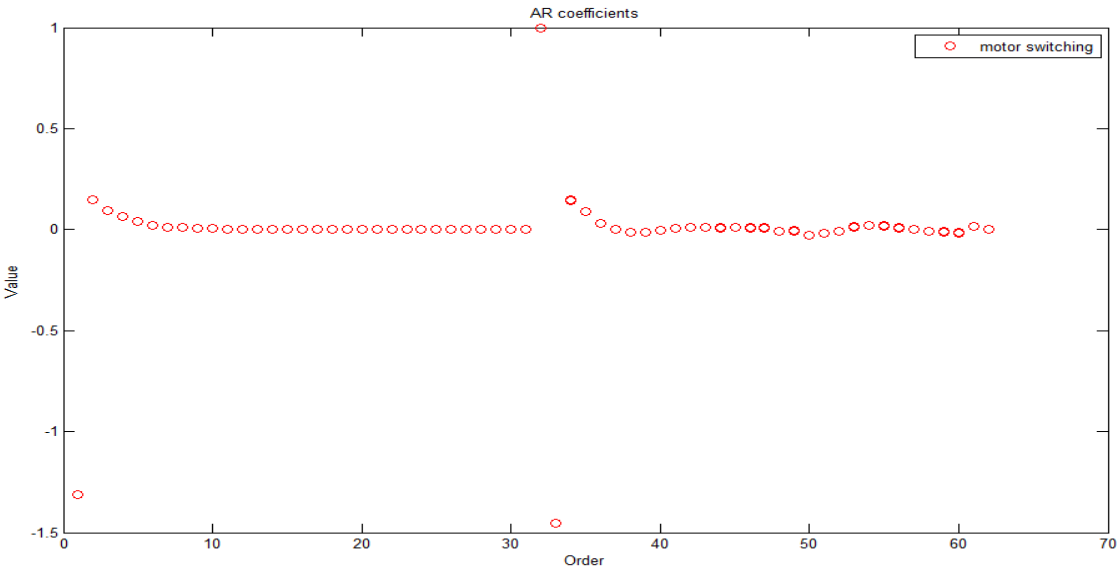


Figure 37 AR Coefficients of the Voltage and Current Signals at PCC for Motor Switching Events

AR modeling as feature extraction tool was able to extract unique representations of the signals and intuitively we may conclude that there is a trend for each event type. However, to distinguish amount the different events, SVM classifier is proposed because using predefined threshold and defining threshold is very difficult to obtain.

### 5.3. Classification

Because of the random nature of the experiment, slight differences may occur between the performances of SVM models for different training/testing data sets. In order to achieve good generalization performances, the training/testing process was repeated ten times by randomly selecting the training/testing data set from the simulated event database using above obtained parameters and procedure shown in Figure 19.

The average prediction error is calculated as a sum of obtained errors divided by the number of iterations. The average error is used to determine generalization error of proposed classifier. The purpose of this step is to evaluate generalization performance of the algorithm on unseen examples.

$$Generalization\ Error = \frac{Error_{Iteration\#1} + \cdots + Error_{Iteration\#N}}{Number\ of\ Iteration\ (N)} \quad (5.1)$$

The overall prediction accuracy for the training data set is estimated to be 100 %, see Table V.

Table V Classification Accuracy on the Training Data Set

| **Cases** | **Training data set prediction accuracy (%)** |
|---|---|
| **Fault Event** | 100 |
| **Capacitor Switching** | 100 |
| **Static Load Switching** | 100 |
| **Motor Load Switching** | 100 |
| **Islanding** | 100 |

Table VI shows classification accuracy for testing data set per event type. In order to analyze performances of the proposed algorithm in detail the test data is separated according to the event type, such as islanding, static load, motor, capacitor and DG switching and fault event. This allows observing how the classifier is performing under each type of the event. The classification error for non-islanding events is 0% and in proves algorithm robustness and insensitivity to the grid faults and switching transients.

The classification accuracy for islanding conditions is estimated to be 98.94%. Table VII summarizes classification accuracy for testing data set. The detail description of the events shown in the Table V and VII may be found in the Table IV.

The overall accuracy of the proposed algorithm is estimated to be 99.49 % with 0.6277% uncertainty. One way of measuring uncertainty is to calculate standard deviation of accuracy across replications of the same experiment:

$$\sigma = \sqrt{\frac{1}{N}\sum_{i=1}^{10}\left(A_i - \mu_{accuracy}\right)^2} \tag{5.2}$$

where

$N$- number of repetitions

$A_i$- detection accuracy for $i^{th}$ repetition

$\mu_{accuracy}$- mean of the detection accuracy

It is evident that prediction accuracy decreases slightly comparing to the training data accuracy and thus it proves good generalization performance of the algorithm. Also, the proposed algorithm shows great robustness in the light loading conditions and impact of the second DG on its operation may be neglected.

Table VI Classification Results per Event Type

| **Cases** | **Testing data set prediction accuracy (%)** |
|---|---|
| **Fault Event** | 100 |
| **Capacitor Switching** | 100 |
| **Static Load Switching** | 100 |
| **Motor Load Switching** | 100 |
| **Islanding** | 98.94 |

Table VII Classification Results for Testing Data Set

| **Cases** | **Prediction Accuracy on the testing data set (%)** |
|---|---|
| **Non-Islanding** | 100 |
| **Islanding** | 98.94 |
| **Total** | 99.49 |

So far the algorithm performances have been tested on the feature vectors that capture transient after its occurrence, the analysis is extended for the feature vectors that contain only part of the transient. The test is performed for the non-islanding events shown in Figure 27-30. The test starts at the transient occurrence and finishes 50ms after the transient occurrence. The 50 ms window slides trough the signals and calculates AR and noise variance coefficients for the each step, then these coefficients are fed into the classifier and predictions are generated.

The Figure. 38-39 show AR coefficients for voltage and current signals for grid fault event shown in Figure 28. In this test the classifier predictions were not affected by partial transient consideration.

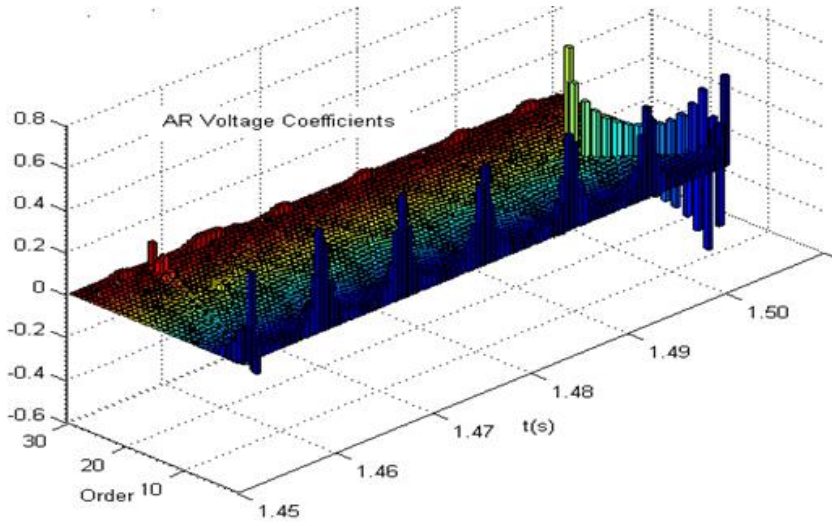


Figure 38 AR Coefficients of the Voltage Signal at PCC for Grid Fault Event

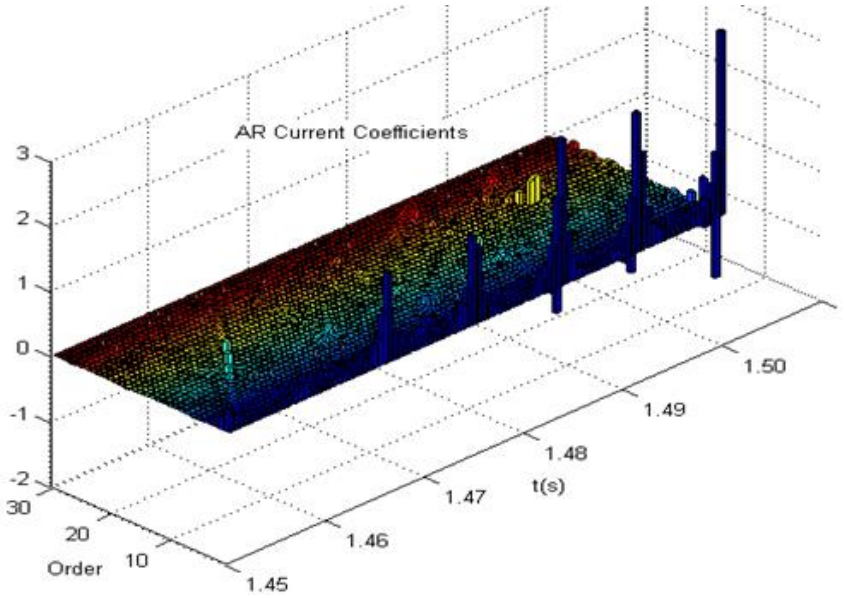


Figure 39 AR Coefficients of the Voltage Signal at PCC for Grid Fault Event

### 5.4. Impact of Data Length on the Classifier Performance

The impact of the data window size on performance of the proposed algorithm is analyzed as well. The algorithm is tested for 10ms, 20ms, 30ms and 40 ms. For these window sizes AR model order $p$=6, 12, 19 and 24 are used to obtain AR coefficients from voltage and current signals. The same procedure described in Figure 6 is utilized. As before, the five-fold cross-validation on the training data set using the simple grid search is performed. And the same values of C=8 and $\gamma = 0.0625$ are shown to be optimal combination of the parameters. The overall prediction accuracy for the training data set is estimated to be 100 %.

The results of this investigation for testing data set and per event type are presented in Table VIII. Table IX shows overall testing accuracy of the proposed method.

Again the algorithm shows high robustness in performance for non-islanding events and miss-operation error for external grid events is estimated to be 0 for all cases. As expected the results clearly show that prediction accuracy decrease with reduction in the window length. Still, performances for the smaller windows have decent classification accuracy and may be applicable in the systems where trade between speed and accuracy should be adjusted towards fast islanding detection.

Table VIII Classification Results for Different Window Sizes

| **Cases** | **Prediction Accuracy on the testing data set (%)** | | | |
|---|---|---|---|---|
| | **10ms** | **20ms** | **30ms** | **40ms** |
| **Fault Event** | 100 | 100 | 100 | 100 |
| **Capacitor Switching** | 100 | 100 | 100 | 100 |
| **Static Load Switching** | 100 | 100 | 100 | 100 |
| **Motor Load Switching** | 100 | 100 | 100 | 100 |
| **Islanding** | 96.96 | 96.96 | 97.12 | 97.71 |

Table IX Classification Results for Testing Data Set

| **Cases** | **Prediction Accuracy on the testing data set (%)** | | | |
|---|---|---|---|---|
| **Non-Islanding** | 100 | 100 | 100 | 100 |
| **Islanding** | 96.96 | 96.96 | 97.12 | 97.71 |
| **Total** | 97.36 | 97.52 | 98.69 | 99.07 |

### 5.5. Implementation Details

The proposed method utilizes 50ms sliding window to extract feature vectors form voltage and current signals at PCC. These vectors are fed into SVM classifier and predictions are made for each step. In case of the islanding trip signal will be sent to the DG switch, Figure 20. to disconnect DG from the grid. The proposed method shows great performances for the active power mismatch up to 40% and reactive power mismatch up to 5% while it may fail to detect islanding for the larger mismatches and therefore it is assumed that this method operates in parallel with Over/Under Voltage (OUV) and Over/Under Frequency (OUF) relays at the PCC. These relays should be set to detect islanding for more than 40% of active and 5% of reactive power mismatches which is high enough to avoid misoperations due to external non-islanding events. OUV

and OUF relays trip fast and accurate in the case of islanding for large power mismatches.

Also, it is important to mention that detection time delay of the proposed method does not depend on the real/reactive power mismatch because the same number of AR parameters, as well as SVM support vectors, is utilized for any event, independently of the real/reactive power mismatch. The detection time delay may be defined as the sum of the time delay caused by AR calculation, which is directly related to the length of the data window, and the number of the SVM support vectors, which is related to the size of the training data set. Therefore, after the training phase, in deployment the delay may be considered constant.

Beside this, the time delay is affected by the speed of the processor. The aim of this study is to show that AR modeling and SVM classifier can be successfully applied for islanding detection and the real time application of the solution have not been analyzed. The SVM model may not be directly applicable in online fashion to big systems, which have several thousand input parameters. In these cases the computational complexity and time delay induced by traditional SVM implementations may grow larger as more data is observed. In those cases, the algorithm improvements, such as compressed kernel [63] or custom hardware improvements [64] will be required. In this study the method is not affected by the SVM computational complexity because the maximum number of the input vectors is 64 but for real time application above mentioned methods may be applicable as well.

## 5.6. Conclusion

In this chapter proposed method performances are evaluated for different islanding and non-islanding events and classification accuracy is estimated. The method shows great robustness to the external events and high classification accuracy for islanding detection of 98.74%. The method is able to determine islanding condition 50 ms after the system disconnection from the main grid. The method shows promising performances on the shorter data windows too. Shorter data windows may be used for the application where trade-off between detection speed and classification accuracy is toward detection speed.

# CHAPTER VI

# CONCLUSION

## 6.1. Summary of Achievements

Due to distributed generation integration into the power system its structure is changing and new challenges arise in the areas of power system protection. To cope with the increased complexity in the power system behavior, new solutions should be characterized by flexibility in protection approach and robustness to the other system transients.

The distribution system is shifting from passive network that transfers power from substation to the customers in a radial fashion to an active network with generation sources. One of the most important requirements for DG safe operation is fast islanding detection. Failure to detect islanding and disconnect the DG may have negative impacts on local devices' operation due to transients during out-of-step reclosing and may pose safety hazard to the utility workers who may touch energized conductors that are being assumed to be dis-energized.

The major contributions of this dissertation are summarized below:

- *Anti-islanding protection*

This study has explored an approach to detect islanding using support vector machine classifier to predict whether the system operates in the islanded mode. A parametric method called the autoregressive modeling is used to extract signal features

from voltage and current measurements at point of common coupling and these coefficients are used as inputs to the SVM classifier. The following conclusions have been reached:

- Autoregressive coefficients of voltage and current signals at point of common coupling have been successfully used as input feature vectors for support vector machine classifier.
- The simulation results show that proposed method has high level of robustness and insensitivity to the external grid disturbances, such as grid faults and component switching events, such as capacitor, motor and load switching events.
- Since proposed method monitors the AR coefficients values for voltage and current measurements, it does not have any negative effect on the power quality.
- The results indicate that this method can detect islanding with a high degree of accuracy of 98.94%
- The proposed method is fast and detection time delay of 50 ms does not depend on the real/reactive power mismatches

## 6.2. Suggestions for Future Work

The research and study in this dissertation may be continued. The following are suggestions for the future work:

- The dependency of the proposed islanding method to the control technique and inverter topology should be investigated. In the future the method's performances may be evaluated for power-voltage control and active-reactive power control technique. Also, the method effectiveness may be tested for the three phase inverter topology.
- Since proposed method utilizes processing of the voltage and current signals and applies classifier to extract signature characteristics for the data classes, the method may be applicable for the power system disturbances detection and classification.
- The detection time delay may be defined as the sum of the time delay caused by AR calculation, which is directly related to the length of the data window, and the number of the SVM support vectors, which is related to the size of the training data set. Beside this, the time delay is affected by the speed of the processor. To improve speed of processing, the algorithm improvements, such as compressed kernel [63] or custom hardware improvements [64] will be required.

# REFERENCES


[1] U. S. A. Federal Energy Regulatory Commission, “Interconnection for Wind Energy, Docket No. RM05-4-000, Order No. 661, Final Rule”, June 2, 2005.

[2] Iov, F.; Hansen, A.D.; Sørensen, P.; Cutululis, N.A., “Mapping of grid faults and grid codes”. Risø-R-1617(EN) (2007) [Online]. Available: http://windenergyresearch.org/2007/01/mapping-of-grid-faults-and-grid-codes/

[3] IEEE Standard for Interconnecting Distributed Resources with Electric Power Systems, IEEE Std 1547-2003, 2003.

[4] Kersting, W.H., "Radial Distribution Test Feeders," Power Engineering Society Winter Meeting, 2001. IEEE , vol.2, no., pp.908,912 vol.2, 2001.

[5] LIBSVM software package. Chih-Wei Hsu, Chih-Jen Lin [Online] Available: http://www.csie.ntu.edu.tw/cjlin/libsvm/. ( June-August 2012)

[6] Lopes, L.A.C.; Huili Sun, "Performance Assessment of Active Frequency Drifting Islanding Detection Methods," Energy Conversion, IEEE Transactions on, vol.21, no.1, pp.171,180, March 2006.

[7] Kern, G. A. "SunSine300: Utility Interactive AC Module Anti-islanding Test Results," 26h IEEE Photovoltaic Specialists Conference, pp.1265,1268, Sep 1997.

[8] Yafaoui, A.; Bin Wu; Kouro, S., "Improved Active Frequency Drift Anti-islanding Detection Method for Grid Connected Photovoltaic Systems," Power Electronics, IEEE Transactions on, vol.27, no.5, pp.2367,2375, May 2012.

[9] Ropp M. E., Begovic M., Rohatgi A., et al. “Determining the Relative Effectiveness of Islanding Detection Methods using Phase Criteria and Non-detection Zones,” Energy Convers, IEEE Transactions on, vol. 15, no. 3, pp. 290,296, Sep. 2000.

[10] Vahedi, H.; Karrari, M., "Adaptive Fuzzy Sandia Frequency-Shift Method for Islanding Protection of Inverter-Based Distributed Generation," Power Delivery, IEEE Transactions on , vol.28, no.1, pp.84,92, Jan. 2013.

[11] Hung G., Chang C., and Chen C., “Automatic Phase-shift Method for Islanding Detection of Grid-connected Photovoltaic Inverter,” Energy Conversion, IEEE Transactions on, vol. 18, no. 1, pp. 169-173, Mar. 2003.

[12] Yuyuma S., Ichinose T., K. Kimoto, et. al“A High Speed Frequency Shift Method as a Protection for Islanding Phenomena of Utility Interactive PV Systems”, Solar Energy Materials, Solar Cells, Vol. 35, Issue 1-4, 1994, pp. 477-486.

[13] Wrinch M. C., “Negative Sequence Impedance Measurement for Distributed Generator Islanding Detection,” Ph.D. dissertation, University of British Columbia, 2008.

[14] Hernandez-Gonzalez G., Iravani R., “Current Injection for Active Islanding Detection of Electronically-interfaced Distributed Resources,” Power Delivery, IEEE Transactions on., vol. 21, no. 3, pp. 1698–1705, Jul. 2006

[15] Cai W., Liu B., Duan S., Zou C., "An Islanding Detection Method Based on Dual-Frequency Harmonic Current Injection Under Grid Impedance Unbalanced

Condition," Industrial Informatics, IEEE Transactions on, vol.9, no.2, pp.1178,1187, May 2013.

[16] Reigosa, D.D.; Briz, F.; Charro, C.B.; Garcia, P.; Guerrero, J.M., "Active Islanding Detection Using High-Frequency Signal Injection," Industry Applications, IEEE Transactions on , vol.48, no.5, pp.1588,1597, Sept.-Oct. 2012.

[17] Jeraputra, C. Enjeti, P.N., "Development of a robust anti-islanding algorithm for utility interconnection of distributed fuel cell powered generation," Power Electronics, IEEE Transactions on , vol.19, no.5, pp. 1163- 1170, Sept. 2004.

[18] Jun Zhang; Dehong Xu; Guoqiao Shen; Ye Zhu; Ning He; Jie Ma, "An Improved Islanding Detection Method for a Grid-Connected Inverter With Intermittent Bilateral Reactive Power Variation," Power Electronics, IEEE Transactions on , vol.28, no.1, pp.268,278, Jan. 2013.

[19] Ye Zhu; Dehong Xu; Ning He; Jie Ma; Jun Zhang; Yangfan Zhang; Guoqiao Shen; Changsheng Hu, "A Novel RPV (Reactive-Power-Variation) Antiislanding Method Based on Adapted Reactive Power Perturbation," Power Electronics, IEEE Transactions on , vol.28, no.11, pp.4998,5012, Nov. 2013.

[20] Ward B., Ropp M. “Evaluation of Islanding Detection Methods for Utility-Interactive Inverters in Photovoltaic Systems”. No. SAND2002-3591. Sandia National Labs., Albuquerque, NM (US); Sandia National Labs., Livermore, CA (US), 2002.

[21] Lopes, L.A.C.; Yongzheng Z. "Islanding Detection Assessment of Multi-Inverter Systems With Active Frequency Drifting Methods," Power Delivery, IEEE Transactions on , vol.23, no.1, pp.480,486, Jan. 2008.

[22] Wang X, Freitas, W.; Dinavahi, V.; Xu, W. "Investigation of Positive Feedback Anti-Islanding Control for Multiple Inverter-Based Distributed Generators," Power Systems, IEEE Transactions on , vol.24, no.2, pp.785,795, May 2009.

[23] Samui A., Samantaray S., "Assessment of ROCPAD Relay for Islanding Detection in Distributed Generation," Smart Grid, IEEE Transactions on, vol. 2, no. 2, pp. 391,398, Jun. 2011.

[24] Stevens J., Bonn R., Ginn J., Gonzalez S., Kern G., "Development and Testing of an Approach to Anti-Islanding in Utility-Interconnected Photovoltaic Systems," Technical Report, Sandia National Laboratories, Albuquerque, NM, August 2000.

[25] Shyh-Jiler H., Fu-Sheng P. 'A New Approach to Islanding Detection of Dispersed Generators with Self-commutated Static Power Converters', Power Delivery, IEEE Transactions on , vol.15, no.2, pp.500,507, Apr 2000.

[26] Danandeh, A.; Seyedi, H.; Babaei, E., "Islanding Detection Using Combined Algorithm Based on Rate of Change of Reactive Power and Current THD Techniques," Power and Energy Engineering Conference (APPEEC), 2012 Asia-Pacific, pp.1,4, 27-29 March 2012.

[27] Jang S., Kim K., "An Islanding Detection Method for Distributed Generations Using Voltage Unbalance and Total Harmonic Distortion of Current," Power Delivery, IEEE Transactions on , vol.19, no.2, pp. 745,752, April 2004.

[28] Salman S., King D.J., Weller G., “Detection of Loss of Mains Based on Using Rate of Change of Voltage and Changes in Power Factor Developments in Power System Protection, 2001, Seventh International Conference on (IEE), pp.82,85, 2001.

[29] Liserre M., Pigazo A., Dell’Aquila A., Moreno V.M.: ‘An Antiislanding Method for Single-phase Inverters Based on a Grid Voltage Sensorless Control’, Industrial Electronics, IEEE Transactions on , vol.53, no.5, pp.1418,1426, Oct. 2006.

[30] Vahedi, H.; Gharehpetian, G.B.; Karrari, M., "Application of Duffing Oscillators for Passive Islanding Detection of Inverter-Based Distributed Generation Units," Power Delivery, IEEE Transactions on , vol.27, no.4, pp.1973,1983, Oct. 2012.

[31] Hsieh C., Lin J., Huang S., “Enhancement of Islanding-detection of Distributed Generation Systems via Wavelet Transform-based Approaches,” International Journal of Electrical Power & Energy Systems, vol. 30, no. 10, pp. 575,580, Dec 2008.

[32] Samui, A.; Samantaray, S. R., "Wavelet Singular Entropy-Based Islanding Detection in Distributed Generation," Power Delivery, IEEE Transactions on , vol.28, no.1, pp.411,418, Jan. 2013.

[33] Bollen M., Gu I.," Signal Processing of Power Quality Disturbances", Wiley-IEEE Press, New York, 2006.

[34] Bishop C.," Pattern Recognition and Machine Learning (Information Science and Statistics)" Springer-Verlag New York Inc, New York, 2006.

[35] Vapnik V., Chervonenkis A.,"Statistical Learning Theory". Wiley, New York, 1998.

[36] Genton M." Classes of Kernels for Machine Learning: A Statistics Perspective" Journal of Machine Learning Research ",vol. 2, pp.299,312 2001.

[37] Najy, W.K.A.; Zeineldin, H.H.; Alaboudy, A.H.K.; Wei Lee Woon; , "A Bayesian Passive Islanding Detection Method for Inverter-Based Distributed Generation Using ESPRIT," Power Delivery, IEEE Transactions on , vol.26, no.4, pp.2687,2696, Oct. 2011

[38] El-Arroudi, K., Joos, G., Kamwa, I.,McGillis, D.T., , "Intelligent-Based Approach to Islanding Detection in Distributed Generation," Power Delivery, IEEE Transactions on , vol.22, no.2, pp.828,835, April 2007.

[39] Madani, S.S.; Abbaspour, A.; Beiraghi, M.; Dehkordi, P.Z.; Ranjbar, A.M., "Islanding Detection for PV and DFIG Using Decision Tree and AdaBoost Algorithm," Innovative Smart Grid Technologies (ISGT Europe), 2012 3rd IEEE PES International Conference and Exhibition on, pp.1,8, 14,17 Oct. 2012.

[40] Dietterich T., "An Experimental Comparison of Three Methods for Constructing Ensembles of Decision Trees: Bagging, Boosting and Randomization", Machine Learning, vol. 40, no.2,pp. 139,158, Aug. 2000.

[41] Lidula, N.W.A., Rajapakse, A.D., "A Pattern-Recognition Approach for Detecting Power Islands Using Transient Signals—Part II: Performance Evaluation", Power Delivery, IEEE Transactions on, vol.27, no.3, pp.1071,1080 July 2012.

[42] Cieslak D, Chawla N, "Learning Decision Trees for Unbalanced Data", European Conference on Machine Learning and Knowledge Discovery in Databases, pp15,19 Sep. 2008.

[43] Samantaray, S. R.; El-Arroudi, K.; Joos, G.; Kamwa, I., "A Fuzzy Rule-Based Approach for Islanding Detection in Distributed Generation," Power Delivery, IEEE Transactions on , vol.25, no.3, pp.1427,1433, July 2010.

[44] Padhee, M.; Dash, P.K.; Krishnanand, K.R.; Rout, P.K.; , "A Fast Gauss-Newton Algorithm for Islanding Detection in Distributed Generation," Smart Grid, IEEE Transactions on , vol.3, no.3, pp.1181,1191, Sept. 2012.

[45] Vapnik. V. " The Nature of Statistical Learning Theory", Springer-Verlag New York Inc, New York, Dec. 1999.

[46] Pigazo, A; Moreno, V.M.; Liserre, M.; Aquila, AD., "Wavelet-Based Islanding Detection Algorithm for Single-Phase Photovoltaic (PV) Distributed Generation Systems," Industrial Electronics, 2007. ISIE 2007. IEEE International Symposium on , pp.2409,2413, June 2007

[47] Akaike,H " On the Likelihood of a Time Series Model", Journal of the Royal Statistical Society. Vol. 27, No. 3/4, pp.217,235, Sep.1978.

[48] Bhansali R., Downham D., “Some Properties of the Order of an Autoregressive Model Selected by a Generalization of Akaike's FPE-criterion “, Biometrika, Vol. 64, No. 3, pp. 547-551,Dec. 1977.

[49] Djuric, P.M., "Asymptotic MAP Criteria for Model Selection," Signal Processing, IEEE Transactions on , vol.46, no.10, pp.2726,2735, Oct 1998.

[50] Jeffreys, H., Jeffreys, B. S. "Weierstrass's Theorem on Approximation by Polynomials and Extension of Weierstrass's Approximation Theory." Methods of Mathematical Physics, 3rd ed. Cambridge University Press, Cambridge, England, pp. 446,448, 1988.

[51] Stoica P., Moses R.” Spectral Analysis of the Signals”, Pearson Prentice Hall, New Jersey, April 2005.

[52] Kiymikb M., Akinc M., Alkanb A. "AR Spectral Analysis of EEG Signals by Using Maximum Likelihood Estimation," Computers in Biology and Medicine 31 vol. 31, no. 6, pp. 441,450, Nov. 2001.

[53] Wies, R.W.; Pierre, J.W.; Trudnowski, D.J., "Use of ARMA Block Processing for Estimating Stationary Low-frequency Electromechanical Modes of Power systems," Power Systems, IEEE Transactions on , vol.18, no.1, pp.167,173, Feb 2003.

[54] Thanagasundram S., Spurgeon S., Schlindwein F."A Fault Detection Tool Using Analysis from an Autoregressive Model Pole Trajectory" Journal of Sound and Vibration ,vol. 317, no. 3, pp. 975,983, Nov. 2008.

[55] Du L., Yang Y., He D., Harley, R.G.; Habetler, T.G.; Lu B., "Support Vector Machine Based Methods for Non-intrusive Identification of Miscellaneous Electric Loads,"38th Annual Conference on IEEE Industrial Electronics Society, pp.4866,4871, Oct. 2012.

[56] Srinivasan, D.; Ng, W. S.; Liew, A.C., "Neural-network-based Signature Recognition for Harmonic Source Identification," Power Delivery, IEEE Transactions on , vol.21, no.1, pp.398,405, Jan. 2006.

[57] Gomez, F.R.; Rajapakse, A.D.; Annakkage, U.D.; Fernando, I.T., "Support Vector Machine-Based Algorithm for Post-Fault Transient Stability Status Prediction Using Synchronized Measurements," Power Systems, IEEE Transactions on , vol.26, no.3, pp.1474,1483, Aug. 2011.

[58] Seethalekshmi, K.; Singh, S.N.; Srivastava, S.C., "A Classification Approach Using Support Vector Machines to Prevent Distance Relay Maloperation Under Power Swing and Voltage Instability," Power Delivery, IEEE Transactions on , vol.27, no.3, pp.1124,1133, July 2012.

[59] Matic-Cuka, B.; Kezunovic, M., "Islanding Detection for Inverter-Based Distributed Generation Using Support Vector Machine Method," Smart Grid, IEEE Transactions on , vol.5, no.6, pp.2676,2686, Nov. 2014.

[60] Bradley E, Tibshirani R.,"An Introduction to the Bootstrap", Chapman & Hall/CRC, Florida, May 1994.

[61] PSCAD/EMTDC [Online] Available: https://hvdc.ca/pscad/ (May 2012)

[62] Teodorescu, R., et al; “Grid Converters for Photovoltaic and Wind Power” Wiley- IEEE Press, New York, Feb 2011.

[63] Cavallanti G., Cesa-Bianchi N., Gentile C., “Tracking the Best Hyperplane with a Simple Budget Perceptron,” Machine Learning, vol.69, no.2, p.143,167, Dec 2007.

[64] Kyrkou, C.; Theocharides, T.; Bouganis, C.-S., "An Embedded Hardware Efficient Architecture for Real-time Cascade Support Vector Machine Classification," Embedded Computer Systems: Architectures, Modeling, and Simulation (SAMOS XIII), 2013 International Conference on, pp.129,136, 15-18 July 2013

# APPENDIX I

Published Papers:


[1] Matic-Cuka, B.; Kezunovic, M., "Islanding Detection for Inverter-Based Distributed Generation Using Support Vector Machine Method," Smart Grid, IEEE Transactions on , vol.5, no.6, pp.2676,2686, Nov. 2014.

[2] Kezunovic M., Matic Cuka B., "Hierarchical Coordinated Protection With High Penetration of Smart Grid Renewable Resources (2.3)," PSerc/DOE Workshop, Madison, WI, May 2013.

[3] Matic-Cuka B, Kezunovic M., "Improving Smart Grid Operation with New Hierarchically Coordinated Protection Approach," MEDPOWER 2012, Cagliari, Italy, October 2012.

[4] Kezunovic M., Matic Cuka B. "Testing and Evaluation of Wind Power Plant Protection System ," ICREPQ'11, Spain, April 2011.

[5] Kezunovic M., Xu F., Matic-Cuka B., Myrda P., "Intelligent Processing of IED Data for Protection Engineers in the Smart Grid," IEEE Mediterranean Electrotechnical Conference (MELECON), Valleta, Malta, April 2010.

[6] Kezunovic M., Myrda P., Matic-Cuka B., "Design of Integrated Analysis Reports Using Data from Substation IEDs," XVI EPRI Substation Equipment Maintenance Optimization and Diagnostics Conference , San Antonio, Texas, March, 2009.

[7] Kezunovic M., Matic-Cuka B., Popovic T., "Substation Data Integration and Utilization," IEEE PES Power Systems Conference and Exposition-PSCE , Seattle, WA, March 2009.

[8] Matic-Cuka B., Kezunovic M., "IED Data Utilization for Operations, Protection, and Maintenance," North American Power Symoposium-NAPS, Calgary, Canada, September, 2008

[9] Kezunovic M., Matic-Cuka B., Gonen O., Badayos N., "An Advanced Data/Information Presentation in Power Systems," ISCA 23rd International Conference on Computers and Their Applications-CATA 08, Cancun, Mexico, April, 2008.

[10] Kezunovic M., Matic-Cuka B., Edris A., "Enterprise-Wide Uses of Diagnostic Data," EPRI Substation Equipment Diagnostics Conference, Tampa, March 2008.